From iron to antibiotics: Identification of conserved bacterial-fungal interactions across diverse partners

Emily C. Pierce[1], Manon Morin[1], Jessica C. Little[2], Roland B. Liu[1], Joanna Tannous[3], Nancy P. Keller[3,4,5], Benjamin E. Wolfe[6], Kit Pogliano[1], Laura M. Sanchez[2], and Rachel J. Dutton[1,7]

1. Division of Biological Sciences, University of California, San Diego, La Jolla, California, USA
2. Department of Pharmaceutical Sciences, College of Pharmacy, University of Illinois at Chicago, Chicago, Illinois, USA
3. Department of Medical Microbiology & Immunology, University of Wisconsin-Madison, Madison, Wisconsin, USA
4. Department of Bacteriology, University of Wisconsin – Madison, Madison, Wisconsin, USA
5. Food Research Institute, University of Wisconsin – Madison, Madison, Wisconsin, USA
6. Department of Biology, Tufts University, Medford, MA, USA
7. Center for Microbiome Innovation, Jacobs School of Engineering, University of California San Diego, La Jolla, United States

ABSTRACT

Microbial interactions are major determinants in shaping microbiome structure and function. Although fungi are found across diverse microbiomes, the mechanisms through which fungi interact with other species remain largely uncharacterized. In this work, we explore the diversity of ways in which fungi can impact bacteria by characterizing interaction mechanisms across 16 different bacterial-fungal pairs, involving 8 different fungi and 2 bacteria (*Escherichia coli* and *Pseudomonas psychrophila*). Using random barcode transposon-site sequencing (RB-TnSeq), we identified a large number of bacterial genes and pathways important in fungal interaction contexts. Within each interaction, fungal partners elicit both antagonistic and beneficial effects. Using a panel of phylogenetically diverse fungi allowed us to identify interactions that were conserved across all species. Our data show that all fungi modulate the availability of iron and biotin, suggesting that these may represent conserved bacterial-fungal interactions. Several fungi also appear to produce previously uncharacterized antibiotic compounds. Generating a mutant in a master regulator of fungal secondary metabolite production showed that fungal metabolites are key shapers of bacterial fitness profiles during interactions. This work demonstrates a diversity of mechanisms through which fungi are able to interact with bacterial species. In addition to many species-specific effects, there appear to be conserved interaction mechanisms which may be important across microbiomes.

INTRODUCTION

Despite awareness that fungi have an immense capacity to produce biologically active metabolites and to reshape ecosystems, fungi are frequently overlooked in microbiome studies in favor of a bacterial-centric focus[1–3]. Recently, fungi and other microeukaryotes have received increased attention in sequencing-based studies[4–9], and there is growing interest in exploring the role fungi and bacterial-fungal interactions play in environmental and host-associated

microbiomes[10–17]. However, the broader patterns and diversity of bacterial-fungal interaction mechanisms have been challenging to characterize given the abiotic and biotic complexity of many microbiomes. While specific interaction mechanisms have been elucidated for particular pairwise bacterial-fungal associations, little is known about the conservation of these mechanisms for other bacterial-fungal pairs and thus about general and widespread interaction mechanisms that could be a major factor in shaping microbiomes.

Fermented foods have been developed as experimentally tractable systems to study multi-kingdom microbial communities[18–20]. Cheese rind biofilms, in particular, represent an ideal system to investigate the diversity and conservation of bacterial-fungal interactions due to the presence of culturable bacterial and fungal species representing diverse phyla. Previous work has shown that biofilms that form on the surface of cheese are composed of an average of six bacterial and three fungal genera[18]. These genera are frequently found in natural and human environments, suggesting that interactions in this system may resemble interspecies interactions in other microbiomes. Communities of isolated fungal and bacterial species from cheese can be reassembled to investigate how these members interact in co-culture[21]. Prior work in this system has demonstrated that fungi in rind biofilms can have both strong positive and negative impacts on bacterial growth and that specialized metabolites can impact these interactions[18,19,22,23].

To systematically characterize the potential effects of fungal species on bacteria within this system, we have employed an interdisciplinary approach. Specifically, we used the high-throughput genetic screen RB-TnSeq[24], RNA-Seq, bacterial cytological profiling, and metabolomics to investigate the diversity of mechanisms through which eight diverse fungal species impact two bacteria (*Escherichia coli* or a cheese-associated *Pseudomonas psychrophila*). A previous study used RB-TnSeq in the cheese rind microbiome system to identify interspecies interactions and to characterize the occurrence of higher-order interactions in a microbial community[21]. RB-TnSeq has been used in other systems to identify genes important for host colonization, to determine essential gene sets, and to characterize genes of unknown function[25–27].

Here, to infer potential mechanisms of bacterial-fungal interactions, we have developed customized experimental and computational RB-TnSeq pipelines to identify genes impacting bacterial fitness in a mixed biofilm with a fungal partner. We observed a diversity of gene functions that affect bacterial fitness in the presence of a fungal partner. Additionally, we found conservation among the impacts of yeasts and filamentous molds on bacteria; a key example of this is the widespread effect on iron metabolism in bacteria, which is mediated by the acquisition of fungal siderophores. Furthermore, we observed similar effects when we expanded our analysis to include soil and skin fungi, suggesting that this mechanism is relevant not only within cheese rind biofilms, but also in other systems. Consistent with the understanding that fungal species have diverse metabolic repertoires, we find several examples of species-specific effects including the apparent production of antimicrobial compounds by filamentous fungal species. Analysis of a fungal mutant defective in secondary metabolite production revealed changes in the bacterial response compared to the wild type (WT) strain, including genes involved in siderophore uptake and antibiotic resistance. This work provides new perspectives on the biology and mechanisms of bacterial-fungal interactions and highlights the key roles of fungi in microbiomes.

RESULTS

Selection of Bacterial-Fungal Interaction Partners

To represent fungal diversity within the cheese environment, we selected a panel of 8 species of commonly found yeasts and filamentous fungi (Figure 1). The selected fungal species from cheese rind microbiomes, which represent five different genera and three fungal classes, include two yeasts, *Candida* sp. str. 135E and *Debaryomyces* sp. str. 135B, and filamentous fungi *Penicillium* sp. str. #12*, Penicillium* sp. str. SAM3*, Penicillium* sp. str. RS17*, Fusarium* sp. str. 554A*, Scopulariopsis* sp. str. JB370, and *Scopulariopsis* sp. str. 165-5. These fungal genera were all present at >1% average abundance in 137 geographically diverse cheese microbiomes analyzed in a previous study of rind diversity[18]. These genera are also found in the human gut mycobiome[28], in the soil[29] , and in marine environments[30].

The bacterial interaction partners selected were two species of Gammaproteobacteria, *Pseudomonas psychrophila* str. JB418 and *Escherichia coli*. We decided to focus on Proteobacteria for this work, as they are common inhabitants of cheese rind communities from diverse geographic locations and have been shown to be responsive to the presence of fungi in experimental community conditions[18] (Supplementary Figure 1 and Supplementary Figure 2). *P. psychrophila* is a native and relatively uncharacterized cheese community member isolated from a Robiola due latti cheese rind. *Pseudomonas* species are of interest not only in cheese, but also in human and soil environments[27,31–33]. *E. coli* was also included as a bacterial partner in this study to take advantage of the vast genetic resources available for this organism. While *E. coli* is not a common member of cheese rind communities, it is relevant both as a causative agent of foodborne illness in cheese and other foods, and as a commensal member of the human gut microbiome that encounters species from consumed fermented foods[34,35].

Characterization of bacterial genes with differential fitness in the presence of fungal partners

Using a pooled library of barcoded transposon-insertion mutants, RB-TnSeq[24] experiments and analyses generate a fitness value for each gene, reflecting the importance of a gene for survival in the experimental condition. Here, we used RB-TnSeq to identify bacterial mutants that have a differential fitness in the presence of a fungal partner compared to growth alone. To do this, we created a modified experimental and computational pipeline that allowed us to measure and quantitatively compare fitness values across multiple conditions. Previous applications of RB-TnSeq have been designed for intra-condition fitness comparisons, allowing the quantitative comparison of fitness values of different genes within a given condition. However, they were not developed for quantitative inter-condition comparisons, which allow the quantitative comparison of fitness values of the same genes between two different conditions. Specifically, additional normalization steps were needed for inter-condition comparisons. Our updated pipeline includes custom R scripts (available at https://github.com/DuttonLab/RB-TnSeq-Microbial-interactions) which provide step-by-step data visualization to follow the progress of data transformation from raw number of reads to normalized fitness values.

Pooled *P. psychrophila*[21] or *E. coli*[24] RB-TnSeq mutant libraries were grown as a lawn for seven days on solid cheese curd agar (CCA) plates[38] either alone or mixed evenly with one of the eight fungal species (Supplementary Figure 3). Mutant abundances at T0 (inoculation) and day 7 were measured via barcode sequencing and differences in barcode abundance were used to calculate gene fitness values within each condition (Supplementary Data 1 and Supplementary Data 2). To identify genes related to interactions, we looked for mutants whose fitness values

were significantly different in a "with fungus" condition versus "alone" condition ($p<0.05$) (Figure 2). We hereafter refer to these differences as an interaction fitness. In some cases, the presence of a fungus increases the fitness of a mutant (positive interaction fitness), whereas in others the fitness of a mutant is decreased (negative interaction fitness).

In total, we found 453 *E. coli* and 692 *P. psychrophila* genes whose disruption leads to fitness alteration in the presence of at least one of the fungal partners used in this study (Supplementary Data 3 and Supplementary Data 4). This represents an average of 163 ± 24 *E. coli* genes per fungal condition and 290 ± 32 *P. psychrophila* genes per fungal condition that have interaction fitness (Figure 3a). These gene sets represent around ten percent of the genes of each bacterium. For *E. coli*, interaction fitness values range from -5.66 to 5.72, and for *P. psychrophila,* -6.18 to 6.02. These values are consistent with previously reported fitness values in other experimental systems, where fitness values greater than 2 and less than -2 are generally thought to represent strong fitness effects[24].

Comparison of interaction fitness across fungal partners

To assess the specificity of interactions, we evaluated the intersections of gene sets across the entire set of fungal interaction conditions (Figure 3b, Supplementary Data 5 and Supplementary Data 6). Many genes show differential fitness only in the presence of specific fungal partners. For *E. coli*, 40 percent of the genes with interaction fitness are specific to a single fungus (n=171), and for *P. psychrophila,* 32 percent (n=219). We also identified a number of genes that had interaction fitness across the entire set of partners (n=30 for *E. coli*, and n=65 for *P. psychrophila*). In addition, around 40 percent (n=269) of the interaction-related genes for *P. psychrophila* and 30 percent (n=137) for *E. coli* were common to at least four of the eight fungal interaction conditions. For both *E. coli* and *P. psychrophila,* growth with *Penicillium* sp. str. #12 and *Penicillium* sp. str. SAM3 results in a large number of the same genes with significant interaction fitness (Figure 3a and Figure 3b). These species also do not cluster with the other fungi in Principal Component Analysis (PCA) of the raw fitness values for all *E. coli* (left) or *P. psychrophila* (right) genes having interaction fitness in at least one fungal condition (Fig 3c).

Mechanisms of fungal impacts on bacterial gene fitness

To identify potential mechanisms underlying bacterial-fungal interactions, we examined the functional distribution of genes associated with interaction fitness. Three functional themes common to multiple fungi used in this study were identified using Clusters of Orthologous Genes (COG) categorization and functional enrichment analysis (Figure 4, Supplementary Data 7 and Supplementary Data 8, Supplementary Figure 4) and analysis of conservation of the effect across fungal species. These interactions include antimicrobial stress on the bacterial cell envelope, competition for biotin, and provision of bioavailable iron.

Penicillium sp. str. #12 and *Penicillium* sp. str. SAM3 induce bacterial envelope stress

Penicillium sp. str. #12 and *Penicillium* sp. str. SAM3 consistently shared impacts on bacterial mutant fitness, as seen by their large number of network connections for both bacteria (Figure 3a and Figure 3b). For *E. coli,* of 116 total genes shared, 22 of these genes are shared

177 only between these two fungi; for *P. psychrophila,* of 187 total genes shared, 19 of these genes
178 are shared only between these two fungi. The gene set shared by these fungi suggests that these
179 two fungal species are producing antibiotic molecules. For *E. coli*, this overlapping gene set
180 includes the genes encoding for the stress protein CspC, beta-lactam antibiotic resistance
181 membrane protein Blr, and the MdtK multidrug efflux pump. Mutants of these genes displayed
182 decreased fitness in the presence of these fungi. This is also supported by the gene set specific to
183 *Penicillium* sp. str. #12*/E.coli,* which includes a regulator of the EmrA multidrug efflux pump
184 and three gene components of the Rcs regulator of capsule synthesis system (*rcsA, rcsC, rcsD*).
185 The Rcs system can respond to damage to the cell envelope and is induced, for example, by
186 membrane-active antimicrobial peptides[40], peptidoglycan damage caused by inhibition of
187 penicillin-binding proteins[41], and mutations in lipopolysaccharide biosynthesis genes[42].
188 Additionally, three genes in the *waa* operon (*waaY, waaP, waaQ)* affecting the modification of
189 the heptose region of the core LPS, which plays a crucial role in membrane stability[43], have
190 increased fitness in the presence of *Penicillium* sp. str. #12. WaaY activity is dependent on WaaP
191 and WaaQ[43]. Inactivation of *waaY* has previously been shown to increase *E. coli*'s resistance to
192 antimicrobial peptide LL-37, due to reduced binding of the peptide to the cell surface[44], and it
193 has also been shown to increase resistance of *Salmonella typhimurium* to antimicrobial
194 peptides[45].
195 When grown in co-culture with *P. psychrophila,* these two fungi induce an interaction
196 fitness for universal stress protein A, whose mRNA is stabilized by the protein encoded by *cspC,*
197 one of the genes with mutants impacted in *E. coli.* With *Penicillium* sp. str. #12*,* three *P.*
198 *psychrophila* genes involved in LPS/lipid A/outer membrane biogenesis (*msbA, arnB, waaG*)
199 also had interaction fitness. While the *P. psychrophila* genome is not as well documented as *E.*
200 *coli*'s, these data are consistent with the *E. coli* data and with the production of antibiotics by
201 these fungi.
202 To investigate fungal antibiotic activity that could be related to the observed changes in
203 bacterial gene fitness, we modified bacterial cytological profiling (BCP) protocols for use on *in*
204 *vitro* cheese biofilms[46]. This microscopy technique was previously developed to rapidly
205 determine the bacterial cellular pathway targeted by antibiotic compounds. We grew wild type
206 (WT) or Δ*mdtK E. coli* alone or in a mixed biofilm with *Penicillium* sp. str. #12 or *Penicillium*
207 sp. str. SAM3 on CCA plates for seven days. Δ*mdtK E. coli* was chosen due to the RB-TnSeq
208 fitness defect of this mutant specifically in the presence of these *Penicillium.* We performed BCP
209 on bacterial cells either co-cultured in the mixed biofilms or after 2 days of growth on CCA
210 plates with known antibiotic compounds as reference controls (Supplementary Figure 5, Figure
211 5). Microscopy showed a strong change in cell morphology for both WT and Δ*mdtK E. coli*
212 when grown with *Penicillium* compared to growth alone (Figure 5). When cultured with these
213 fungi, *E coli* cells exhibit a rounded phenotype, consistent with a reduction in cell wall integrity
214 and reminiscent of cells treated with antibiotics that target cell wall biosynthesis such as
215 mecillinam and amoxicillin. Δ*mdtK* cells are strongly affected and have spheroplasted, indicative
216 of the complete loss of structural integrity. Neither of these two fungal strains are known
217 producers of penicillin, and analysis of the *Penicillium* sp. str. #12 draft genome failed to detect
218 penicillin biosynthesis gene clusters[47]. However, these BCP results are consistent with our RB-
219 TnSeq data and suggest that these two fungal strains are inducing stress on the bacterial cell
220 envelope through an undetermined mechanism that may involve novel antimicrobials.

221 Fungi increase bacterial need for biotin biosynthesis

222 *Pseudomonas* interaction fitness genes suggested competition for environmental biotin
223 between *P. psychrophila* and all of the studied fungal partners. Biotin, found in both milk and
224 cheese[48], is present in our cheese curd agar medium at 73 nmol/mg and represents an essential
225 cofactor for enzymes involved in key cellular functions like amino acid metabolism and lipid
226 synthesis[49]. Three *P. psychrophila* genes associated with biotin biosynthesis mutants (*bioB,*
227 *bioD, bioF*) have a negative interaction fitness in the presence of all eight fungi. An additional
228 three genes are associated with a negative interaction fitness in the presence of seven fungi
229 (*bioA, bioC, bioH*) (Figure 4). The biotin biosynthesis pathway was also significantly enriched
230 with fungal partners in functional enrichment analysis of interaction fitness gene sets
231 (Supplementary Data 8). Additionally, differential expression analysis from RNA-Seq of *E. coli*
232 grown either alone or in the presence of *Penicillium* sp. str. #12 showed that *bioA, bioB, bioC,*
233 *bioD,* and *bioF* were all significantly upregulated in the presence of the fungus with an average
234 fold change of 4.4 (Supplementary Data 9). This highlights an increased need for bacterial biotin
235 synthesis, which again supports that fungi and bacteria are consistently competing for available
236 biotin in the medium, or potentially that bacteria have higher biotin requirements in the presence
237 of fungi. Although some species of fungi are capable of biotin biosynthesis, others are capable of
238 only partial synthesis or are incapable[50]. Notably, this interaction appears to be conserved across
239 both bacteria and all fungi.

240 Fungi increase iron availability for bacterial community members

241 Because iron is essential for bacterial growth and cheese is an iron-limited environment,
242 with free iron levels measured to be approximately 3 ppm, microbial species growing on cheese
243 require iron chelators with specific transport systems to sustain their growth[21,51–53]. Our RB-
244 TnSeq fitness data revealed that *E. coli* mutants defective in enterobactin transport grow better in
245 the presence of all fungal partners than they do alone (Figure 4, Figure 6a). These genes include
246 members of the *fep* operon (*fepC, fepG, fepA*), which encodes enterobactin transport functions,
247 and *exbD,* which encodes a component of an iron-siderophore transport complex. In most fungal
248 conditions, mutants in an enterobactin esterase encoded by *fes* in addition to iron-siderophore
249 related transport genes *fepB, fepD, tonB* and *exbB* also grow better in the presence of a fungal
250 partner. When grown with any fungal partner, ferric-enterobactin transport is significantly
251 enriched among all the functions associated with genes that have an interaction fitness
252 (Supplementary Data 7).
253 For *P. psychrophila,* we noticed two genes that have a strong fitness defect alone, but
254 positive interaction fitness when any fungus is present. These genes, Ga0212129_114259 (avg.
255 interaction fitness 3.3) and Ga0212129_114260 (avg. interaction fitness 5.3) are annotated as
256 uncharacterized protein DUF3649 and as an uncharacterized iron-regulated membrane protein.
257 The protein encoded by Ga0212129_114259 is 99% identical to an iron transporter from
258 *Pseudomonas fragi* (NCBI Protein Accession WP_133145017.1). Moreover, immediately
259 upstream of these two genes we find a ferric enterobactin receptor (fepA) and the PfeR-PfeS
260 two-component regulatory system required for production of the ferric enterobactin receptor,
261 suggesting that this region may be involved in siderophore uptake. Again, positive interaction
262 fitness for these likely siderophore-uptake associated genes suggests that possibly more iron is
263 available for *P. psychrophila* when fungi are present.

264 To validate the RB-TnSeq results related to the Fep system genes, we performed
265 competitive mutant fitness assays with a 1:1 ratio of WT *E. coli* and Δ*fepC,* Δ*fepA,* and Δ*fepG*
266 mutants either alone or in the presence of *Scopulariopsis* sp. str. JB370 or *Penicillium* sp. str.
267 #12. When no fungus is present, there is a clear growth defect for Δ*fep* mutants. After 7 days,
268 both Δ*fepA* and Δ*fepG* mutants grew significantly better with both fungi, whereas there was no
269 difference in wild-type growth with or without fungus. The Δ*fepC* mutant grew significantly
270 better with *Penicillium* sp. str. #12 (Figure 6b).
271 Additionally, differential expression analysis from RNA-Seq of *E. coli* grown on CCA
272 for three days either alone or in the presence of *Penicillium* sp. str. #12 revealed 34 genes (out of
273 a total of 348 significantly upregulated genes) involved in iron acquisition that are specifically
274 upregulated in the presence of the fungus (Supplementary Data 10). Notably, we find genes
275 associated with the uptake machinery for hydroxamate siderophores (including *fhuA* and *fhuE*),
276 which are commonly produced by fungi. We also observe upregulation of enterobactin
277 biosynthesis and uptake, suggesting that *E. coli*, even in the presence of fungi, still produces and
278 utilizes its native siderophore, enterobactin (Figure 6c).
279 All filamentous molds in this study, but not yeast, produce siderophores that were
280 detectable by liquid Chrome Azurol S (CAS) assay (Supplementary Figure 6). Given the positive
281 CAS assays, we next sought to identify the siderophores produced by these fungal species. We
282 performed liquid chromatography mass spectrometry (LC-MS and LC-MS/MS) for all fungal
283 species. This metabolomics data showed evidence of the hydroxamate fungal siderophores
284 coprogen and ferrichrome in *Fusarium* and *Penicillium* species (Figure 6d). Although not
285 detected in these extracts, *Scopulariopsis* sp. str. JB370 is predicted to make dimethylcoprogen
286 based on antiSMASH analysis of the draft genome[54].
287 We hypothesized that the increased fitness of enterobactin *fep* mutants was due to the
288 uptake of fungal siderophores through an alternate pathway. Indeed, we found that coprogen and
289 ferrichrome can rescue the growth defect of Δ*fepA* and Δ*fepC* on CCA (Figure 6e). The *E. coli*
290 Fhu system has previously been shown to allow uptake of hydroxamate-type siderophores[55–58].
291 In *E. coli,* ferrichrome uptake is known to be mediated by the outer membrane receptor FhuA,
292 and coprogen uptake is mediated by the outer membrane receptor FhuE. Mutants of *fhuA* or *fhuE*
293 alone do not show a growth defect on CCA, likely because the enterobactin system is intact.
294 Thus, to specifically examine fungal siderophore uptake, we constructed mutants of *fhuA* or *fhuE*
295 in an enterobactin-uptake defective background. Δ*fepA*Δ*fhuA,* Δ*fepA*Δ*fhuE,* and Δ*fepC*Δ*fhuE*
296 were grown on CCA in the presence or absence of fungal siderophores (Figure 6e). Combined
297 loss of enterobactin uptake and *fhuA* eliminates the alleviation seen with ferrichrome, whereas
298 loss of either *fhuA* or *fhuE* in the Δ*fepA* background seems to eliminate the alleviation seen with
299 coprogen. This suggests that *E. coli* requires *fhuA* for ferrichrome uptake, and both *fhuA* and
300 *fhuE* for coprogen uptake.
301 To validate that the fungi used in this study are alleviating *E. coli's* need for enterobactin
302 through the same mechanism, equal volumes of WT or Δ*fep*/Δ*fhu* mutants were spotted on CCA
303 at varying distances from a pre-cultured fungal front (Figure 6f, Supplementary Figure 7).
304 Growth of Δ*fepA* and Δ*fepC* is restored closest to the fungal fronts of all filamentous molds, but
305 not yeast species. For *Penicillium* sp. str. #12, *Scopulariopsis* sp. str. JB370, and *Scopulariopsis*
306 sp. str. 165-5, this effect is lost in the Δ*fepA*Δ*fhuE* and Δ*fepC*Δ*fhuE* double mutant, suggesting it
307 is *fhuE*-dependent. For *Fusarium* sp. str. 554A and *Penicillium* sp. str. RS17*,* it is both *fhuE* and
308 *fhuA*-dependent. For *Penicillium* sp. str. SAM3, loss of *fhuA* decreases but does not eliminate
309 alleviation. Thus, we can conclude that near a fungal partner, *E. coli* is likely to use and benefit

310 from fungal hydroxamate siderophores that are taken up by the FhuA and FhuE uptake systems
311 independently of the enterobactin uptake system.
312 Given that iron limitation is a common challenge across many environments, we wanted
313 to examine whether fungal species from other ecosystems could also be producing siderophores
314 accessible to neighboring bacterial species. We performed similar assays with *Aspergillus*
315 *fumigatus,* a soil-dwelling filamentous ascomycete that was originally isolated from the lung
316 tissue of a patient who had aspergillosis[59]. This assay was also performed for *Malassezia*
317 *pachydermatis,* a yeast commensal resident on animal skin. *M. pachydermatis* is also sometimes
318 found on human skin and can act as an opportunistic pathogen; this species has caused
319 bloodstream infections in hospitalized neonates[60,61]. Interestingly, Δ*fepA*Δ*fhuE* and Δ*fepC*Δ*fhuE*
320 mutants are rescued next to *A. fumigatus*, whereas the Δ*fepA*Δ*fhuA* mutant lacking the
321 ferrichrome receptor was not, suggesting that *A. fumigatus* produces a siderophore capable of
322 being imported through FhuA (Figure 6f). *A. fumigatus* is known to produce the extracellular
323 siderophores fusarinine C and triacetylfusarinine C, which are not known to be imported via the
324 Fhu system, and the intracellular siderophore ferricrocin, which is similar to ferrichrome but not
325 expected to be excreted[62]. Ultimately, it is unclear what siderophore is responsible for the effects
326 by *A. fumigatus*. We see a similar effect using *M. pachydermatis,* suggesting that bacteria are
327 able to utilize siderophores from a yeast species using the Fhu system (Figure 6f). *Malassezia*
328 *restricta* and *Malassezia globosa* have previously been found to possess genes for siderophore
329 biosynthesis[63,64]. We performed AntiSMASH[54] analysis on a previously published genome of
330 this *Malassezia pachydermatis* strain, and were able to identify a NRPS biosynthetic gene cluster
331 containing a ferrichrome peptide synthetase[54,65,66]. In sum, our results suggest that diverse fungi
332 can reduce bacterial dependence on their own siderophores by secreting xenosiderophores.

333 **Loss of a fungal secondary metabolite regulator alters the profile of interaction fitness**

334

335 The cases above show that bacterial gene fitness can be impacted by the production of
336 fungal secondary metabolites, including antimicrobial compounds and siderophores. Previous
337 studies have shown that fungal secondary metabolite production is regulated by the master
338 regulator, LaeA[67]. Loss of LaeA in *Aspergillus* spp., *Fusarium oxysporum,* and *Penicillium*
339 *chrysogenum* is associated with loss of secondary metabolite production[68,69]. To test the impact
340 of alterations in fungal metabolite production on bacterial gene fitness, we generated a Δ*laeA*
341 mutant in *Penicillium* sp. str. #12.
342 To assess the impact of the *laeA* knockout on fungal metabolites in *Penicillium* sp. str.
343 #12, we performed RNA-Seq and liquid chromatography with mass spectrometry (LC-MS) on
344 the WT and *ΔlaeA* mutant. Fourteen percent of the genome (1925 out of 13261 genes) was
345 differentially expressed between WT and *ΔlaeA* (Figure 7a, Supplementary Data 11). This is
346 consistent with previous findings in *A. fumigatus* that LaeA influenced expression of around 10
347 percent of the fungal genome[67]. GO term enrichment analysis identified melanin, organic
348 hydroxy compound, phenol-containing compound, pigment, sterigmatocystin, depsipeptide,
349 lactone, mycotoxin, and organic heteropentacyclic compound biosynthesis as pathways
350 overrepresented in in the set of 1070 genes more expressed in WT (Supplementary Data 12).
351 Among the genes more expressed in WT, we find four genes in a nonribosomal peptide
352 synthetase cluster region predicted by AntiSMASH[54]; these four genes have homology to *sid2,*
353 *sidF, sidH*, and *sitT,* genes associated with siderophore biosynthesis and transport in

354 *Aspergillus*[62]. This gene cluster also includes genes with homology to *sidJ* and *mirB,* providing
355 further evidence that this region has a siderophore-related function. Five genes in a predicted
356 gene cluster encoding production of serinocyclin A and four genes in a predicted cluster
357 encoding production of nidulanin A are also more highly expressed in WT than in *ΔlaeA.* All
358 together, this confirms that deletion of *laeA* is likely to reduce production of fungal secondary
359 metabolites including siderophores. Among the 855 genes more expressed in *ΔlaeA,* GO term
360 enrichment identified amino acid and nucleoside metabolism, fungal cell wall, and ion transport
361 (Supplementary Data 12), highlighting a possible reorganization of *Penicillium* sp. str. #12
362 metabolism in the absence of *laeA*.
363 LC-MS comparison of the two extracts showed differential production of many
364 metabolites, 94 of which have a >10-fold change between the two (Supplementary Data 13). Of
365 these, 93 are less abundant in the *ΔlaeA* mutant, which is consistent with the loss of secondary
366 metabolite production in the *ΔlaeA* mutant (Figure 7b). Some of these metabolites matched with
367 known secondary metabolites and their analogs based on mass and fragmentation pattern.
368 Namely, atlantinone A and cyclopenol were found to be produced by the WT *Penicillium* sp. str.
369 #12 in >10-fold higher quantity than the *ΔlaeA* mutant, and pyripyropene O was putatively
370 identified and produced in >2-fold higher quantity. Cyclopenol is an alkaloid that is described as
371 a mycotoxin in the benzodiazepine class[70] and serves as an biosynthetic intermediate for
372 viridicatol[71], which has been described as having antibacterial activity against *Staphylococcus*
373 *aureus*[72]. Small amounts of viridicatol were indeed found in extracts with high quantities of
374 cyclopenol. Atlantinone A is a meroterpenoid that is derived from the same biosynthetic pathway
375 as other mixed polyketide-terpenoids such as andrastins and citrehybridones produced by various
376 *Penicillium* and *Aspergillus* species[73]. Both pyripyropene O and atlantinone A have tested
377 negative for antimicrobial activity when screened against a panel of bacteria, including an *E. coli*
378 strain[74,75]. The ecological role of these metabolites remains undetermined. In combination with
379 our RNA-Seq analysis, these data highlight an important diminution of secondary metabolite
380 production in the *ΔlaeA* strain.
381 We next performed RB-TnSeq experiments with the *Penicillium* sp. str. #12 Δ*laeA*
382 mutant to determine whether this single fungal mutation leads to changes in the genes needed for
383 bacterial fitness. While some interaction fitnesses are preserved between Δ*laeA* and WT, loss of
384 LaeA appears to significantly change the profile of interactions (Figure 7c). As LaeA is predicted
385 to impact siderophore production, we would expect that *E. coli* enterobactin uptake mutants
386 would not be as strongly impacted by the presence of the Δ*laeA* mutant. Although we see
387 positive interaction fitness of *fepA*, *fepB*, *fepC* and *fepG* genes when E. coli is grown with WT
388 *Penicillium* sp. str. #12 relative to *E. coli* growth alone, we do not see positive interaction fitness
389 of *fep* genes with Δ*laeA Penicillium* sp. str. #12 (Supplementary Data 14). Indeed, liquid CAS
390 assays demonstrate that this mutant produces less siderophores than WT on cheese media (Figure
391 7d). Together, these data support the hypothesis that loss of a fungal secondary metabolite
392 regulator corresponds to changes in bacterial interaction fitness effects.
393 Our RB-TnSeq results, combined with the antibiotic assay BCP, suggested that
394 antibiotic activity by *Penicillium* sp. str. #12 causes damage to *E. coli*'s cell envelope. As the
395 *laeA* mutant should have a decreased ability to produce antimicrobial compounds, we examined
396 whether there were changes in the fitness of genes related to responses to antibiotics. The *mdtK*
397 efflux pump gene, which was previously seen to have negative interaction fitness when grown
398 with WT *Penicillium* sp. str. #12, no longer has an interaction fitness with Δ*laeA*, suggesting that
399 the Δ*laeA* mutant has decreased antibiotic production. Although the exact nature of the

400 antimicrobials produced by this strain is unknown, these results are consistent with previous
401 studies, which show that LaeA regulates antibiotic production in other fungal species, and with
402 our metabolite analysis, which showed a decrease in production of many metabolites in Δ*laeA*.
403 Overall, these findings suggest that a single fungal gene can strongly impact the bacterial genes
404 needed for fitness and in particular point out that fungal specialized metabolite production may
405 play a large role in determination of bacterial fitness in bacterial-fungal interactions.

406 **DISCUSSION**

407 Fungi have been shown to strongly impact bacterial neighbors in diverse systems, from
408 soil to polymicrobial infections[77–85]. To characterize the effects of fungi from a simple
409 microbiome on bacteria, we used a high-throughput genetic screen, RB-TnSeq, to identify
410 bacterial genes relevant to fungal interactions. We observed a diversity of interactions, in terms
411 of direction (+/-), strength, and mechanism. These mechanisms include effects on important
412 cellular pathways such as biotin synthesis and antibiotic resistance. Our work demonstrates that
413 there is both a large diversity of bacterial-fungal interactions as well as conservation of key
414 interaction mechanisms across different fungi.
415 One of the strongest and most widespread bacterial-fungal interactions that we observed
416 suggests that fungal species can dramatically modulate access to iron through the provision of
417 fungal siderophores, such as ferrichrome and coprogen. Although it has long been known that
418 bacteria grown in isolation are able to uptake purified fungal siderophores[55,56], our results
419 demonstrate that this exchange takes place between bacteria and fungi growing in a biofilm and
420 that this exchange can have impacts on the competitive fitness of bacteria.
421 Hydroxamate siderophore receptors homologous to FhuE and FhuA are widespread in
422 Proteobacteria, suggesting that this interkingdom siderophore transfer may play an important role
423 in altering metal availability in diverse systems. *Pseudomonas aeruginosa* has previously been
424 shown to produce phenazine metabolites that led to upregulation of extracellular siderophore
425 production by *A. fumigatus*[86]. Fhu uptake systems have also been identified in the Gram-positive
426 bacterial pathogens *Streptococcus agalactiae* and *Listeria monocytogenes*, and growth of non-
427 siderophore producing mutants of *Streptomyces coelicolor* was restored by the presence of
428 siderophores from airborne contaminant fungi[87–90]. Additionally, hydroxamate siderophore
429 uptake systems have been shown to impact *Staphylococcus aureus* fitness in a murine infection
430 model[91]. Another study has shown that the presence of a siderophore-producing, cheese-
431 associated *Scopulariopsis* produced siderophores and caused downregulation of siderophore
432 production by *Staphylococcus equorum*[52]. *Bacteroides fragilis,* a human gut symbiont, is also
433 able to use ferrichrome to grow in iron-limiting conditions, and *fhu* genes are expressed by *E.*
434 *coli* in colonic mucus[92,93]. Some fungi consumed as a part of fermented foods have been shown
435 to survive digestive system transit, and fermented foods are known to contain fungal
436 siderophores[94,95], which could be a source of fungal siderophores in the gut in addition to
437 potential siderophore production by gut-resident species[94–96]. All together, these results suggest
438 that bacterial use of fungal siderophores may be a widespread mechanism of interkingdom
439 interaction. Considering the crucial role of iron acquisition and metabolism in microbial survival,
440 this conserved interaction mechanism could be a determinant in shaping environmental and host-
441 associated microbiomes.
442 This study provides new insight into the wide range of fungal impacts on bacteria that
443 can occur even in a simple microbiome. Our data also suggest that even among Proteobacteria,

444 fungal impacts may be diverse. Of the 692 *P. psychrophila* genes and 453 *E. coli* genes that had
445 an interaction fitness with at least one fungal partner, only 58 were homologous based on
446 BLAST (Supplementary Data 15). Further, many genes with interaction fitness do not have a
447 known function. We anticipated that by looking for fungal impacts on *E. coli,* we could leverage
448 the vastly superior genetic information available for this species. However, even in this well-
449 characterized organism, 43% of genes identified as having interaction fitness are annotated as
450 hypothetical or putative. For *P. psychrophila,* 29% of genes with interaction fitness are
451 hypothetical proteins. This highlights that many genes involved in interspecies interactions might
452 yet to be characterized, and that studying microbes in the context of their interactions with other
453 species, and not just in monoculture, provides an avenue for uncovering new areas of biology.
454
455
456 **MATERIALS AND METHODS**

457 Fungal Ribosomal RNA Sequencing

458 Genomic DNA was extracted with phenol-chloroform (pH 8) from cultures of the eight cheese
459 fungal species used in this study. For each extraction: 125 µL of 425–600 µm acid-washed beads
460 and 125 µL of 150–212 µm acid-washed beads were poured in a screw-capped 2 mL tube. 500
461 µL of 2X buffer B (200 mM NaCl, 20 mM EDTA) and 210 µL of SDS 20% were added to the
462 tube containing fungal material and 500 µL of Phenol:Chloroform (pH 8). Cells were lysed by
463 vortexing the tubes for 2 min at maximum speed. Aqueous and organic phases were separated by
464 centrifugation at 4°C, 8,000 RPM for 3 min and 450 µL of the aqueous phase (upper phase) were
465 recovered in a 1.5 mL Eppendorf tube. 45 µL of sodium acetate 3M and 450 µL of ice cold
466 isopropanol were added before incubating the tubes at −80°C for 10 min. The tubes were then
467 centrifuged for 5 min at 4°C at 13,000 RPM. The pellet was then washed in 750 µL of 70% ice
468 cold ethanol and re-suspended in 50 µL of DNase/RNase free water. Following DNA extraction,
469 LROR (ACCCGCTGAACTTAAGC) and LR6 (CGCCAGTTCTGCTTACC)[97] primers were
470 used to amplify the large subunit of the ribosomal RNA and for *Penicillium* species, Bt2a
471 (GGTAACCAAATCGGTGCTGCTTTC) Bt2b (ACCCTCAGTGTAGTGACCCTTGGC)[98]
472 primers were used to amplify the beta-tubulin gene. PCR was performed in a final volume of 50
473 µL: 25 µL of Q5 polymerase master mix (New England Biolabs), 2.5 µL of the forward primer
474 at 10 µM, 2.5 µL of the reverse primer at 10 µM, 100 ng of genomic DNA, and water using the
475 following PCR programs: LSU-(i) 98°C - 30 s, (ii) 35 cycles of: 98°C – 10 s; 52°C – 30 s; 72°C
476 – 1.5 min, (iii) 72°C – 5 min; Beta-tubulin-(i) 98°C - 30 s, (ii) 35 cycles of: 98°C – 10 s; 57°C –
477 30 s; 72°C – 1 min, (iii) 72°C – 5 min. PCR products were purified with the QIAquick PCR
478 purification kit (Qiagen) and sequenced using the forward and reverse primer by Eton Bioscience
479 Inc. (San Diego, USA). Consensus sequences from forward and reverse sequencing reactions
480 were aligned using Geneious version R9 9.1.8 (http://www.geneious.com). The MrBayes[36]
481 plugin for Geneious was used to build the phylogenetic tree with the following parameters:
482 Substitution model- JC69; Rate variation- gamma; Outgroup- *Fusarium* sp. str. 554A; Gamma
483 categories-4; Chain Length- 1100000; Subsampling freq- 200; Heated chains-4; Burn-in length-
484 100000; Heated chain temp- 0.2; Random seed-1160; Unconstrained branch lengths- 1, 0.1, 1, 1.
485 FigTree v1.4.4 was used for visualization (https://github.com/rambaut/figtree/releases).
486
487 Bacterial-Fungal Growth Assays

488 We aimed to inoculate 60,000 bacterial cells alone or with 6,000 fungal spores per well on 10%
489 CCA medium[38] adjusted to pH 7 in a 96-well plate. Each bacterial or bacterial-fungal assay was
490 done in triplicate. After 7 days of growth, the entire well was harvested and homogenized in
491 PBS1X-Tween 0.05% prior to dilution and plating on LB with 20 µg/ml cycloheximide (for
492 bacterial counts) or milk plate count agar with 50 µg/ml chloramphenicol (for fungal spore
493 counts). Counts were done at inoculation and after harvest. Final growth counts were then
494 compared in co-culture condition relative to growth alone to identify interaction impacts.
495 Significant growth impacts were determined based on Dunnett's test[99], p-value < 0.05. Plots
496 were made with R package ggplot2 3.2.1[100].

497 Microbial Culturing for LC-MS/MS extraction

498 All fungal cultures were grown on plate count agar milk salt (PCAMS; 1 g/L whole milk
499 powder, 1 g/L dextrose, 2.5 g/L yeast extract, 5 g/L tryptone, 10 g/L sodium chloride, 15 g/L
500 agar). Plates were kept at room temperature and spores were harvested at 7 days of growth (or
501 after sporulation was observed) for subsequent experiments. Spores harvested from fungi were
502 put into PBS and normalized to an OD_{600} of 0.1 for working stock.

503 Extraction of cultures

504 Three biological replicates of each condition were plated (distinct samples) and extracted from
505 solid agar. For extraction from solid agar plates, 5 µL of fungal working stock were spotted onto
506 10% CCA medium adjusted to pH 7. Following 7 days of growth, agar was removed from the
507 Petri dish and placed into 50 mL falcon tubes. Acetonitrile (10 mL) was added to each tube and
508 all were sonicated for 30 minutes. All falcon tubes were centrifuged and liquid was removed
509 from the solid agar pieces and transferred to 15 mL falcon tubes. The 15 mL falcon tubes
510 containing liquid were then centrifuged and liquid was again removed from any residual solid
511 debris and transferred to glass scintillation vials. These liquid extractions were then dried *in*
512 *vacuo*. Dried extracts were weighed and diluted with MeOH to obtain 1 mg/mL solutions which
513 were stored at -20°C until analysis via LC-MS/MS.

514 LC-MS/MS data collection

515 High resolution LC-MS and LC-MS/MS data were collected on a Bruker impact II qTOF in
516 positive mode with the detection window set from 50 to 1500 Da, on a 2.1x150mm C18 cortecs
517 UPLC column with a flow rate of 0.5mL/min for a gradient of 10-100% ACN with 0.1% formic
518 acid over 16 minutes. For each sample, 10 μL of a 1mg/mL solution was injected. The ESI
519 conditions were set with the capillary voltage at 4.5 kV. For MS^2, dynamic exclusion was used,
520 and the top nine precursor ions from each MS^1 scan were subjected to collision energies scaled
521 according to mass and charge state for a total of nine data dependent MS^2 events per MS^1. MS^2
522 data for pooled biological replicates is deposited under MassIVE accession number
523 MSV000085070. MS^1 and MS^2 data for *ΔlaeA* and WT *Penicillium* sp. str. #12 is deposited
524 under MassIVE accession number MSV000085054 and was collected under identical conditions
525 on a Bruker compact qTOF.

526 Molecular Networking

527 For all extractions, all precursor *m/z*'s that were found in solvent and agar controls (based on
528 both retention time and mass tolerance) were removed prior to input into GNPS using the
529 BLANKA algorithm.[101] A molecular network (
530 https://gnps.ucsd.edu/ProteoSAFe/status.jsp?task=464b331ef9d54de9957d23b4f9b9db14) was
531 created using the online workflow at GNPS. The data was filtered by removing all MS/MS peaks
532 within +/- 17 Da of the precursor *m/z*. MS/MS spectra were window filtered by choosing only
533 the top 6 peaks in the +/- 50Da window throughout the spectrum. The data was then clustered
534 with MS-Cluster with a parent mass tolerance of .02 Da and a MS/MS fragment ion tolerance of
535 .02 Da to create consensus spectra. Further, consensus spectra that contained less than 2 spectra
536 were discarded. A network was then created where edges were filtered to have a cosine score
537 above 0.7 and more than 6 matched peaks. Further edges between two nodes were kept in the
538 network if and only if each of the nodes appeared in each other's respective top 10 most similar
539 nodes. The spectra in the network were then searched against GNPS' spectral libraries. The
540 library spectra were filtered in the same manner as the input data. All matches kept between
541 network spectra and library spectra were required to have a score above 0.7 and at least 6
542 matched peaks. Solvent and agar control files were also loaded into the networks in order to
543 perform removal based on fragmentation patterns. All nodes with precursor masses less than
544 200Da were also removed. The extensive background and low *m/z* Da removal was done to more
545 accurately reflect the metabolomic profiles of fungal genera in an attempt to represent only true
546 metabolites. The DEREPLICATOR was used to annotate MS/MS spectra[102,103]. The molecular
547 networks were visualized using Cytoscape software[104].

548 RB-TnSeq Assays

549 All RB-TnSeq assays were performed on 10% CCA medium adjusted to pH 7. Prior to
550 inoculation, one aliquot of each library was thawed and inoculated into 25 mL of liquid LB-
551 kanamycin (50 µg/mL). Once the culture reached mid-log phase (OD = 0.6–0.8), 5 mL of that
552 pre-culture was pelleted and stored at −80°C for the T0 reference in the fitness analysis. The
553 remaining cells were used to inoculate the fitness assay conditions. For each RB-TnSeq fitness
554 assay, we aimed to inoculate 7,000,000 cells of the bacterial library (on average 50 cells per
555 insertion mutant). For fitness assays including a fungal partner, 700,000 fungal cells were
556 inoculated based on spore counts. Pre-cultured cells were washed in PBS1X-Tween 0.05%,
557 mixed with appropriate volumes of quantified fungal spore stocks, and then inoculated by
558 spreading evenly on a 100 mm petri dish containing 10% CCA medium, pH 7. For each
559 condition, assays were performed in triplicate (3 distinct samples). After seven days, each plate
560 was flooded with 1.5 mL of PBS1X-Tween 0.05% and cells were scraped off, taking care to not
561 disturb the CCA. The liquid was then transferred into a 1.5 mL microfuge tube and cells were
562 pelleted by centrifugation. After removing the supernatant, the cells were washed in 1 mL of
563 RNAprotect solution (Qiagen, Hilden, Germany), pelleted and stored at −80°C until gDNA
564 extraction. Genomic DNA was extracted with phenol-chloroform (pH 8) using the same protocol
565 used for fungal gDNA extraction described above. Samples were stored at −80°C until further
566 analysis.
567 After gDNA extraction, extracts containing Penicillium sp. str. #12 DNA were purified
568 using the OneStep PCR Inhibitor Removal Kit (Zymo Research, CA, USA). Then, the 98°C
569 BarSeq PCR as described in Wetmore *et al*., 2015[24] was used to amplify only the barcoded

570 region of the transposons. PCR was performed in a final volume of 50 µL: 25 µL of Q5
571 polymerase master mix (New England Biolabs, MA, USA), 10 µL of GC enhancer buffer (New
572 England Biolabs), 2.5 µL of the common reverse primer (BarSeq_P1 – Wetmore et al., 2015) at
573 10 µM, 2.5 µL of a forward primer from the 96 forward primers (BarSeq_P2_ITXXX) at 10 µM
574 and either 200 ng of gDNA for alone conditions, or 2 µg of gDNA for fungal interaction
575 conditions. For *E. coli* analysis, we performed 84 PCRs (T0 sample and 28 harvest samples in
576 triplicate) involving 28 different multiplexing indexes. For *P. psychrophila* JB418 analysis, we
577 performed 84 PCRs (T0 sample and 28 harvest samples in triplicate) involving 28 different
578 multiplexing indexes. We used the following PCR program: (i) 98°C - 4 min, (ii) 30 cycles of:
579 98°C – 30 s; 55°C – 30 s; 72°C – 30 s, (iii) 72°C – 5 min. After the PCR, for both *E. coli* and *P.*
580 *psychrophila,* 10 µL of each of the PCR products were pooled together to create the BarSeq
581 sequencing library and 200 µL of the pooled library were purified using the MinElute
582 purification kit (Qiagen, Germany). The final elution of the BarSeq library was performed in 30
583 µL in DNase and RNase free water. The BarSeq libraries were then quantified using Qubit
584 dsDNA HS assay kit (Invitrogen, CA, USA) and sequenced on HiSeq4000 (75 bp, single-end
585 reads), by the IGM Genomics Center at the University of California San Diego. The sequencing
586 depth for each condition varied between 6.1 and 11.7 million reads for *E. coli* and 5.8 and 13.3
587 million reads for *P. psychrophila.*

588 RB-TnSeq Data Processing

589 Custom R scripts were used to determine the average fitness scores for each gene across three
590 RB-TnSeq assay replicates. These scripts are available at https://github.com/DuttonLab/RB-
591 TnSeq-Microbial-interactions. The Readme document provides an in-depth explanation of all
592 data processing steps performed in these scripts. In brief, insertion mutants that did not have a
593 sufficient T0 count (3) in each condition or that are not centrally inserted (10-90% of gene) were
594 removed from analysis. Counts determined by Wetmore *et al*.[24] scripts were then normalized to a
595 reference gene (*allB* in *E. coli* and closest protein BLAST match Ga0212129_11710 in *P.*
596 *psychrophila*) to be able to compare across conditions and to account for differences in
597 sequencing depth. These genes do not have a strong fitness effect in any condition based on
598 former fitness determination developed by Wetmore *et al.*, 2015[24]. Un-normalized strain fitness
599 was then calculated per insertion mutant as the log2 of the ratio of the corrected counts in the
600 condition and the corrected counts in the T0 sample. Un-normalized gene fitness and variance
601 was next calculated by averaging insertion mutants within a gene. These values were then
602 normalized based on the position of the gene along the chromosome, as well as by the mean of
603 the data distribution. These steps were all done on individual replicates. Next, the average gene
604 fitness and associated variance were calculated using the weighted average of the fitness values
605 across the three different replicates. Then, for each condition, fitness values are corrected by the
606 mean of the replicate means (the replicate means being the mean values used to center fitness
607 value within a replicate). Finally, based on the assumption that most genes should have no fitness
608 effect, we corrected gene fitness values in each condition by the mode (peak of the density
609 distribution). Final fitness values were then compared for fungal interaction conditions compared
610 to bacterial alone conditions and comparisons associated with a p-value lower than 5% were
611 considered significant interaction fitness (alpha parameter=0.05 in
612 2conditions_FitnessComparison.R code). Networks of fitness values were visualized in
613 Cytoscape v. 3.5.1[104] and PCA plots were made with R package ggplot2 3.2.1[100] and ggfortify

614 0.4.7[105]. COG category mapping of *E. coli* and *P. psychrophila* protein sequences was done by
615 eggNOG-mapper v2[106] and visualized with R package ggplot2 3.2.1[100].

616 Bacterial Cytological Profiling

617 Approximately 7,000,000 WT *E. coli* K-12 strain BW25113 or Keio collection *mdtK* mutant
618 cells[107] were inoculated alone or co-inoculated with 700,000 *Penicillium* sp. str. #12 or
619 *Penicillium* sp. str. SAM3 spores on 10% CCA pH 7. After 7 days of growth, 1 mL of T-Base
620 buffer was added to the surface of the biofilms, and biofilms were scraped into the buffer. For
621 co-culture conditions, the sample was filtered through a 0.5 µm filter to specifically remove
622 fungal material. 2 µL of concentrated dye mix (1 µL 1 mg/mL FM4-64, 1 µL 2 mg/mL DAPI in
623 48 µL T-Base) were added to 20 µL of filtrate. Dye-filtrate mix was spotted onto agarose-LB
624 pads (1% Agarose, 20% LB liquid medium, 80% ddH_2O) and imaged by fluorescence and phase
625 contrast. Control compound references on CCA medium were obtained by spotting 30 µL of 5x,
626 10x, 25x, and 100x MIC dilutions of antibiotics onto quadrants on CCA medium pH 7 plates,
627 allowing to dry, and spread-plating 200 µL of log-phase (OD 0.1) *E. coli* cultures. After two
628 days of growth, cells near the edge of the zone of inhibition on appropriate dilution spots were
629 resuspended in 10 µL of prediluted dye mix (1 µL 1 mg/mL FM4-64, 1 µL 2 mg/mL DAPI in
630 998 µL T-Base) and spotted onto agarose-LB pads and imaged as described above. Resulting
631 images were deconvolved using Deltavision SoftWorx software (Applied Precision, Inc., WA,
632 USA), analyzed using Fiji[108], and assembled in Adobe Photoshop (Adobe, CA, USA).

633 CCA medium biotin quantification

634 Biotin quantification of CCA medium was performed on three replicate samples by Creative
635 Proteomics (NY, USA) as follows: 100 mg of each sample was homogenized in water (10
636 µL/mg) for 1 min three times with the aid of 5-mm metal balls on a MM400 mill mixer.
637 Methanol at 10 µL/mg was then added. Water-soluble vitamins were extracted by vortex-mixing
638 for 2 min and sonication in a water batch for 5 min. After centrifugation, the clear supernatants
639 were cleaned up by solid-phase extraction on a Strata-X (60 mg/mL) cartridge. The eluted
640 fractions containing water-soluble vitamins were collected, pooled and then dried under a gentle
641 nitrogen gas flow in a nitrogen evaporator. The residues were dissolved in 200 µL of 10%
642 methanol. Twenty microliter aliquots were injected to run UPLC-MRM/MS with the use of a
643 C18 UPLC column and with (+) ion detection and (-) ion detection, respectively. Calibration
644 curves were prepared by injection of serially-diluted mixed standard solutions of water-soluble
645 vitamins. Concentrations of detected vitamins were calculated by interpolating the linear
646 calibration curves.

647 Δ*fep* mutant competitive growth assays

648 Approximately 600,000 WT and Δ*fepA,* Δ*fepC,* or Δ*fepG* Keio collection[107] mutant cells were
649 inoculated at a 1:1 ratio either alone or co-inoculated with approximately 60,000 *Penicillium* sp.
650 str. #12 or *Scopulariopsis* sp. str. JB370 spores on 10% CCA pH 7 in a 96-well plate in four
651 replicates each (4 distinct samples). After seven days of growth, the entire well was harvested
652 and homogenized in PBS1X-Tween 0.05% prior to dilution and plating on LB with 20 µg/ml
653 cycloheximide (total bacterial counts) or with 20 µg/ml cycloheximide and 50 µg/ml kanamycin
654 (bacterial mutant counts). Final growth counts were then compared in co-culture condition

655 relative to growth alone to identify interaction impacts. Significant growth impacts were
656 determined by significantly different growth in the presence of a fungus relative to growth alone
657 based on a two-sided two-sample equal variance t-test p-value < 0.05. Plots made with R
658 package ggplot2 3.2.1[100].

659

660 RNA-Seq and differential expression analysis of *E. coli* with *Penicillium* sp. str. #12

661 Approximately 7,000,000 *E. coli* cells were inoculated in triplicate (3 distinct samples) either
662 alone or with approximately 700,000 *Penicillium* sp. str. #12 spores on 10% CCA pH 7. After 3
663 days, the biofilms were harvested for RNA extraction and washed with 1 mL of RNAprotect.
664 RNA was extracted by a phenol-chloroform extraction (pH 8) using the same extraction protocol
665 as for gDNA extraction. Extractions were then purified with the OneStep PCR Inhibitor
666 Removal Kit (Zymo Research, CA, USA).
667 Sequencing libraries were prepared as follows. RNA samples were treated with DNase
668 using the 'Rigorous DNase treatment' for the Turbo DNA-free kit (AMBION, Life
669 Technologies, Waltham, MA, USA) and RNA concentration was measured by nucleic acid
670 quantification in Epoch Microplate Spectrophotometer (BioTek, Winooski, VT, USA). Transfer
671 RNAs and 5S RNA were then removed using the MEGAclear Kit Purification for Large Scale
672 Transcription Reactions (AMBION, Life Technologies) following manufacturer instructions.
673 Absence of tRNA and 5S RNA was verified by running 100 ng of RNA on a 1.5% agarose gel
674 and RNA concentration was quantified by nucleic acid quantification in Epoch Microplate
675 Spectrophotometer. Also, presence of gDNA was assessed by PCR using universal bacterial 16S
676 PCR primers (Forward primer: AGAGTTTGATCCTGGCTCAG, Reverse Primer:
677 GGTTACCTTGTTACGACTT). The PCR was performed in a final volume of 20 µL: 10 µL of
678 Q5 polymerase master mix (New England Biolabs), 0.5 µL of forward primer 10 uM, 0.5 µL of
679 reverse primer 10 uM and 5 µL of non-diluted RNA. PCR products were run on a 1.7% agarose
680 gel and if gDNA was amplified, another DNase treatment was performed as well as a new
681 verification of absence of gDNA.
682 Ribosomal RNA depletion was performed using the RiboMinus Transcriptome Isolation
683 Kit (Yeast and Bacteria) for the *E. coli* alone samples and using both the RiboMinus
684 Transcriptome Isolation Kit (Yeast and Bacteria) and the RiboMinus Eukaryote Kit v2 for the
685 mixed *E. coli/Penicillium* sp. str. #12 samples (ThermoFisher Scientific). For the *E. coli* alone
686 samples, each sample was divided into two for treatment and then repooled for RNA recovery
687 with ethanol precipitation. For the *E. coli/Penicillium* sp. str. #12 samples, an equal volume of
688 the eukaryotic probe and RiboMinus Bacterial Probe Mix were used to deplete both bacterial and
689 fungal ribosomal RNA and RNA was recovered with ethanol precipitation. Concentrations after
690 ribosomal RNA depletion were measured using Qubit RNA HS Assay Kits (Invitrogen). The
691 RNA-Seq library was produced using the NEBNext Ultra RNA Library Prep Kit for Illumina for
692 purified mRNA or ribosome-depleted RNA. We prepared a library with a fragment size of 300
693 nucleotides and used the 10 µM NEBNext Multiplex Oligos for Illumina (Set 1, NEB #E7335)
694 lot 0091412 and the NEBNext multiplex Oligos for Illumina (Set 2, NEB #E7500) lot 0071412.
695 We performed PCR product purification with 0.8X Agencourt AMPure XP Beads. Library
696 samples were quantified with Qubit DNA HS Assay Kits before the quality and fragment size
697 were validated by TapeStation (HiSensD1000 ScreenTape). Library samples were pooled at a
698 concentration of 15 nM each and were sequenced on HiSeq4000 (50 bp, single-end). TapeStation

699 assays and sequencing were performed by the IGM Genomics Center at the University of
700 California San Diego.
701 Following sequencing, reads were mapped to the concatenated genome of *E. coli* K12
702 BW25113[109] and *Penicillium* sp. str. #12 using Geneious version R9 9.1.8
703 (http://www.geneious.com). Only the reads that uniquely mapped to a single location on the *E.*
704 *coli* genome section were kept. *E. coli* expression analysis was performed using the following R
705 packages: Rsamtools (R package version 2.0.3), GenomeInfoDb (R package version 1.20.0),
706 GenomicFeatures[110] (R package version 1.36.4), GenomicAlignments[110] (R package version
707 1.20.1), GenomicRanges[110] (R package version 1.36.1) and DESeq2[111] (R package version
708 1.20.1). We followed the workflow described by Love *et al*. and performed the differential
709 expression analysis using the package DESeq2. Differentially expressed genes between two
710 conditions were selected with an adjusted p-value lower than 5% (Benjamini-Hochberg
711 correction for multiple testing) and an absolute log2 of fold change equal to or greater than 1.5.

712 Construction of *E. coli* mutants and visual interaction assays

713 Visual assays for hydroxamate siderophore stimulation:

714 Antibiotic assay discs (Whatman) were placed on CCA medium pH 7 with .005% tetrazolium
715 chloride (an indicator of cellular respiration) and 20 µL of water, 10 µM coprogen or ferrichrome
716 (EMC Microcollections GmbH) solutions (in water) were slowly pipetted onto the disc and
717 allowed to absorb. 2.5 µL of 37°C overnight LB cultures of *E. coli* K12 BW25113 WT, Δ*fepA,*
718 Δ*fepC,* Δ*fhuE,* Δ*fhuA,* Δ*fepA*Δ*fhuE,* Δ*fepC*Δ*fhuE,* or Δ*fepA*Δ*fhuA* mutants[107] were spotted next
719 to the discs. Double mutants were constructed as described below. Plates were left at room
720 temperature until red color developed.

721 Visual assays for fungal stimulation of bacterial mutants:

722 Fungal spores were inoculated on CCA pH 7 with .005% tetrazolium chloride. After fungal
723 growth at room temperature (cheese fungal isolates) or 30°C (*A. fumigatus* and *M.*
724 *pachydermatis*), 2.5 µL of *E. coli* 37°C overnight LB cultures were spotted at increasing
725 distances from the fungal front. Plates were left at room temperature until red color developed. *A.*
726 *fumigatus* isolate AF293 was received from Nancy Keller, University of Wisconsin-Madison. *M.*
727 *pachydermatis* was originally isolated from the ear of a dog in Sweden (ATCC14522).

728 Creation of Δ*fepA*Δ*fhuE* and Δ*fepC*Δ*fhuE*:

729 Chemically competent cells for Δ*fepA* or Δ*fepC* mutants were created. An overnight culture of
730 Δ*fepA* or Δ*fepC* mutants was diluted 1:100 and grown at 37°C until OD 0.4-0.6. The culture was
731 placed on ice for 20 minutes and then centrifuged at 4°C for 10 minutes at 6000 rpm to collect
732 the cells. Supernatant was removed and cells were resuspended in half the previous volume of
733 pre-cooled 0.1M $CaCl_2$. After being left on ice for 30 minutes, centrifugation was repeated and
734 supernatant was removed before resuspension in a quarter of the original volume of pre-cooled
735 0.1M $CaCl_2$/15% glycerol. Cells were aliquoted and stored at -80°C until transformation. These
736 cells were transformed with the pKD46 plasmid [112], recovered at 30°C and plated on LB plates
737 with 100 µg/mL Ampicillin and grown at 30°C. Overnight cultures were started from individual
738 colonies for creation of electrocompetent cells. Overnight cultures of Δ*fepC*-pkD46 or Δ*fepA*-
739 pkD46 were diluted 1:100 in fresh LB- 100 µg/mL Ampicillin and grown at 30°C until an OD of
740 0.1. 20 µL of fresh 1 M L-arabinose were added and growth was continued at 30°C until OD 0.4-
741 0.6. Cells were then chilled on ice for 15 minutes and then centrifuged for ten minutes at 4000

742 rcf 4°C. Cells were resuspended in 1 mL of ice water and centrifuged for ten minutes at 4000 rcf
743 at 4°C. Cells were resuspended in 0.5 mL of ice water and centrifuged for ten minutes at 4000 rcf
744 4°C. Cells were resuspended in 50 µL of ice water and kept on ice until transformation. The
745 chloramphenicol resistance cassette was amplified from the pKD3 plasmid [112] using the custom
746 primers: FhuEcatF
747 (CAGATGGCTGCCTTTTTTACAGGTGTTATTCAGAATTGATACGTGCCGGTAATGGCG
748 CGCCTTACGCCCC) and FhuEcatR
749 (CCTCCTCCGGCATGAGCCTGACGACAACATAAACCAAGAGATTTCAAATGCTGGGC
750 CAACTTTTGGCGAA) and the following PCR conditions (i) 98°C - 30 sec, (ii) 30 cycles of:
751 98°C – 10 s; 70°C – 20 s; 72°C – 30 s, (iii) 72°C – 5 min. Amplification was performed on 4 ng
752 of pKD3 plasmid using Q5 High-Fidelity 2X Master Mix (New England Biolabs). The PCR
753 product was digested for 1 hour with the restriction enzymes DpnI and ClaI at 37°C and then the
754 PCR product was run on a 1% agarose gel. The PCR product was extracted using the QIAquick
755 Gel Extraction Kit (Qiagen) and then dialyzed for 4 hours with TE buffer. 1.5 µL of dialyzed
756 PCR product was used to transform the electrocompetent Δ*fepC*-pkD46 or Δ*fepA*-pkD46 cells.
757 After 2 hours of recovery in SOC medium with 1mM arabinose at 37°C, the transformation was
758 plated on LB with 50 mg/mL kanamycin and chloramphenicol. Transformants were confirmed
759 to be Δ*fhuE* with Eton Bioscience Inc. sequencing of the chloramphenicol cassette.

760 Creation of Δ*fepA*Δ*fhuA:*

761 Creation was done as with Δ*fepA*Δ*fhuE,* except that the chloramphenicol resistance cassette was
762 amplified from pKD3[112] using FhuAcatF (ATCATTCTCGTTTACGTTATCATTCACTTT
763 ACATCAGAGATATACCAATGAATGGCGCGCCTTACGCCCCAATGGCGCGCCTTACG
764 CCCC) and FhuAcatR
765 (GCACGGAAATCCGTGCCCCAAAAGAGAAATTAGAAACGGAAGGTTGCGGTCTGGG
766 CCAACTTTTGGCGAACTGGGCCAACTTTTGGCGAA) custom primers.

767 *Penicillium* sp. str. #12 genome sequencing, assembly, and annotation

768 Genomic DNA was extracted from *Penicillium* sp. str. #12 using the genomic DNA extraction
769 protocol described above. High molecular weight DNA (average 16 Kb) was sequenced on the
770 Oxford Nanopore MinION with a R.9.5 flow cell using $1D^2$ sequencing adaptors from kit SQK-
771 LSK308 (Oxford Nanopore Technologies, Oxford, United Kingdom). Raw data was basecalled
772 using guppy 3.3.0 (Oxford Nanopore Technologies, Oxford, United Kingdom)(guppy_basecaller
773 -config dna_r9.5_450bps.cfg --fast5_out) for 1D basecalls and these were used to also obtain
774 higher accuracy 1D^2 basecalls (guppy_basecaller_1d2 -i 1Dbasecall/workspace/ --config
775 dba_r9.5_450bps_1d2_raw.cfg --index_file 1Dbasecall/sequencing_summary.txt) These reads
776 were assembled by canu 1.8[113] and polished by racon 1.4.3[114] four times and by pilon 1.23[115]
777 once. The final assembly is 38 Mbp and consists of 52 contigs.

778 *Penicillium* sp. str. #12 genome annotations were obtained by combining genomic and
779 transcriptomic information from RNA-Seq. To obtain the gene expression profile of *Penicillium*
780 sp. str. #12, approximately 700,000 WT *Penicillium* sp. str. #12 spores were inoculated in
781 triplicate on 10% CCA pH 7. After 3 days, the biofilms were harvested for RNA extraction and
782 washed with 1mL of RNAprotect. RNA was extracted and RNA-Seq libraries were prepared as
783 described above with the following modification: Ribosomal RNA depletion was performed
784 using the RiboMinus Eukaryote Kit v1 and RNA was recovered with ethanol precipitation. After

785 sequencing, the RNA-Seq reads from these *Penicillium* sp. str. #12 alone cultures were
786 concatenated with RNA-Seq reads from the previously described *E. coli/Penicillium* sp. str. #12
787 co-culture conditions that uniquely mapped to a single location on the *Penicillium* sp. str. #12
788 genome. The full set of transcriptomic reads were then used as input into the FunGAP annotation
789 pipeline and 77 million of these reads mapped[116]. This pipeline predicted 13261 protein-coding
790 genes in the *Penicillium* sp. str. #12 genome. Interproscan[117] was used within the FunGAP
791 pipeline for function prediction of genes. This Whole Genome Shotgun project has been
792 deposited at DDBJ/ENA/GenBank under the accession JAASRZ000000000. The version
793 described in this paper is version JAASRZ010000000.

794 Creation and confirmation of *laeA* deletion in *Penicillium* sp. str. #12

795

796 Deletion cassette design strategy*:* In order to knockout *laeA* in *Penicillium* sp. str. #12, the
797 isolate was first screened for hygromycin and phleomycin resistance. *Penicillium* sp. str. #12
798 showed a confirmed sensitivity to both antibiotics. A three round PCR deletion strategy was used
799 to replace the *laeA* ORF with the *hph* gene, whose expression confers selection on
800 hygromycin[118]. The schematic representation of the *laeA* gene replacement with the hph gene is
801 depicted in Supplementary Figure 8. The deletion cassette (5'flank- hph- 3'flank) was
802 constructed using three sequential PCR reactions. In the first PCR round, about 1 Kb genomic
803 sequence flanking either the 5' or 3' end of the *laeA* ORF were amplified using the primer sets
804 P12_KOlaeA_5' F (CTCCGTTGGGCCCTCAC) and 5'R
805 (GCAATTTAACTGTGATAAACTACCGCATTAAAGCTGTTGATATCGGCAATCAATCA
806 ATG) or P12_KOlaeA_3'F
807 (GGTGGGCCTTGACATGTGCAGCCGGTGGAGCGGCGCCTGGTGAATCCTACCCACAT
808 GG) and 3'R (CGTTGGGAGGAAAAGCTTCTGCG) respectively. The *hph* gene was amplified
809 from plasmid pUCH2-8 using primers hph_F (AGCTTTAATGCGGTAGTTTATCACAG) and
810 hph_R (CTCCACCGGCTGCACATGTC). A second PCR reaction was performed to assemble
811 by homologous recombination the three individual fragments from the first round PCR. The
812 deletion cassettes were finally amplified using the nested primer set, P12_KOlaeA_NestedF
813 (CAGACGGTCCGCATCCCG) and P12_KOlaeA_NestedR
814 (GGTCCAGGTGCAGTAGTACTG).
815
816 Fungal transformation*:* To generate the deletion strains, a protoplast-mediated transformation
817 protocol was employed. Briefly, 109 fresh spores were cultured in 500 mL of liquid minimal
818 medium (LMM) for 12 h under 25°C and 280 rpm. Newly born hyphae were harvested by
819 centrifugation at 8000 rpm for 15 min and hydrolyzed in a mixture of 30 mg Lysing Enzyme
820 from Trichoderma (Sigma-Aldrich) and 20 mg Yatalase (Fisher Scientific) in 10 mL of Osmotic
821 Medium (1.2 M $MgSO_4$, 10 mM NaPB, pH 5.8). The quality of protoplast was monitored under
822 the microscope after four hours of shaking under 28 °C and 80 rpm. The protoplast mixture was
823 later overlaid with 10 mL of trapping buffer (0.6 M sorbitol, 100 mM Tris-HCl pH 7.0) and
824 centrifuged for 15 min under 4°C and 5000 rpm. Protoplasts were collected from the interface,
825 overlaid with an equal volume of STC (1.2 M sorbitol, 10 mM Tris-HCL pH 7.5,10 mM $CaCl_2$)
826 and decanted by centrifugation at 6000 rpm for 8 min. The protoplast pellet was resuspended in
827 500 µL STC and used for transformation. After 5 days of incubation at 25 °C, colonies grown on
828 stabilized minimal medium (SMM) plates supplemented with hygromycin were subjected to a

second round of selection on hygromycin plates. In total, 25 hygromycin-resistant transformants were isolated after a rapid screening procedure on SMM supplemented with hygromycin. Single-spored transformants were later tested for proper homologous recombination at the ORF locus by PCR and Southern blot analysis.

Gene-deletion strain confirmation*:* The correct replacement of the *laeA* with the *hph* gene was first verified by PCR analysis of genomic DNA derived from the transformant strains using primer set P12_laeA_F (CACAATGGCTGAACACTCTCGG) and P12_laeA_R (GGGATATGGAGCATCGAAGTTGC) that amplify the *laeA* ORF. About 12% (3/25) of the monoconidial lines generated from primary transformants of *Penicillium* sp. str. #12 were PCR-positive for the absence of the *laeA* ORF. The positive deletion strains were further checked for a single insertion of the deletion cassette by Southern blot analysis and revealed single-site integration of the deletion cassette in one transformant (Supplementary Figure 8). Probes corresponding to the 5' and 3' flanks of the *laeA* gene in each strain were labeled using [α32P] dCTP (PerkinElmer, USA) following the manufacturer's instructions.

RNA-Seq analysis of WT and Δ*laeA Penicillium* sp. str. #12

To characterize the effect of the *laeA* deletion on the *Penicillium* sp. str. #12 gene expression profile, we performed RNA-Seq analysis for Δ*laeA Penicillium* sp. str. #12. As for WT *Penicillium* sp. str. #12, 700,000 Δ*laeA Penicillium* sp. str. #12 spores were inoculated in triplicate (3 distinct samples) on 10% CCA pH 7 and biofilms were harvested after 3 days. Harvest, RNA extraction and library preparation were performed identically to WT *Penicillium* sp. str. #12. Then, *Penicillium* sp. str. #12 and Δ*laeA* differential expression analysis was performed as described for *E. coli/Penicillium* sp. str. #12 above. To look for enrichment of functions in the set of differentially expressed genes, we input the protein sequences of the genes into the gene-list enrichment function of KOBAS 3.0[119]. Sequences were searched against the Gene Ontology (GO) database[120,121] using *A. fumigatus* as a reference for GO assignment before conducting a hypergeometric test with Benjamini-Hochberg correction. Functions with a corrected p-value <.05 were considered enriched.

Data Availability

Sequence data that support the findings of this study (RB-TnSeq, RNA-Seq) have been deposited in the NCBI SRA database with BioProject PRJNA624168. Mass spectrometry data is available in the MassIVE database under accession numbers MSV000085070 and MSV000085054. The GNPS molecular network is available at https://gnps.ucsd.edu/ProteoSAFe/status.jsp?task=464b331ef9d54de9957d23b4f9b9db14. The Whole Genome Shotgun project for *Penicillium* sp. str. #12 has been deposited at DDBJ/ENA/GenBank under the accession JAASRZ000000000 in BioProject PRJNA612335. The version described in this paper is version JAASRZ010000000. In addition to these sources, source data used to create figures 2,3,4, 6, and 7 is available in the Supplementary Data provided with the paper.

Code Availability

The R scripts developed for processing RB-TnSeq data described in this manuscript are available at https://github.com/DuttonLab/RB-TnSeq-Microbial-interactions along with usage instructions.

874 The perl scripts needed for initial processing of RB-TnSeq data published in Wetmore *et al.*
875 2015[24] are available at https://bitbucket.org/berkeleylab/feba/src/master/.
876
877 Availability of biological materials
878 All unique materials, including described fungal strains isolated from cheese, the *P. psychrophila*
879 JB418 strain and RB-TnSeq library, *laeA Penicillium* sp. str. #12 deletion mutant, and *E. coli*
880 siderophore uptake double mutants, are readily available from the authors upon request. The *E.*
881 *coli* RB-TnSeq library and Keio strains can be requested from the groups that created these
882 resources (PMID references provided). *Penicillium* sp. str. SAM3 is commercially available from
883 Danisco.
884

Resource Sources			
Resource	**Source or reference**	**Identifiers**	**Additional information**
Keio collection, strain background *Escherichia coli* K12	PMID: 16738554	CGSC, RRID:SCR_002303	Collection of 3,818 *E. coli* knockout strains
Keio_ML9 library, strain background *Escherichia coli* K12	PMID: 25968644		RB-TnSeq library of *E. coli* K12 BW25113 (152,018 pooled insertion mutants)
JB418_ECP1 library, strain background *Pseudomonas psychrophila* JB418	PMID: 30211673		RB-TnSeq library generated in the *P. psychrophila* JB418 strain isolated from cheese (272,329 pooled insertion mutants)
Keio ME9062, strain background *Escherichia coli* K12	PMID: 16738554	CGSC#: 7636	Parent strain of the Keio collection mutants
Penicillium sp. str. SAM3	Danisco - CHOOZIT	PC SAM 3 LYO 10D	Industrial starter for cheese production
Pseudomonas psychrophila JB418	PMID: 30211673		Strain isolated from Robiola due latti cheese
Candida sp. str. 135E	This paper		Strain isolated from cheese
Debaryomyces sp. str. 135B	This paper		Strain isolated from cheese
Penicillium sp. str. #12	This paper		Strain isolated from cheese
Penicillium sp. str. RS17	This paper		Strain isolated from cheese
Scopulariopsis sp. str. JB370	This paper		Strain isolated from cheese
Scopulariopsis sp. str. 165-5	This paper		Strain isolated from cheese
Fusarium sp. str. 554A	This paper		Strain isolated from cheese
Aspergillus fumigatus str. AF293	Nancy Keller, University of Wisconsin-Madison		
Malassezia pachydermatis str. CBS 1879	ATCC14522		

885

886

887 **ACKNOWLEDGMENTS**

888 The authors would like to thank: the Arkin lab and the Deutschbauer lab at UC-Berkeley for the
889 *E. coli* Keio_ML9 library, Kristen Jepsen at the IGM Genomics Center at the University of
890 California San Diego for assistance with sequencing, Dr. Sergey Kryazhimskiy (UCSD) for his
891 input on RB-TnSeq data processing, Cong Dinh (UCSD) for assistance with fungal genome
892 assembly, William Bushnell for assistance with fitness validation experiments, Dr. Sinem
893 Beyhan for advice on fungal genome annotation, Lisa Marotz (UCSD) for assistance with non-
894 cheese yeasts, and members of the Dutton lab, especially Brooke Anderson, for constructive
895 comments on the manuscript.
896
897 **FUNDING SOURCES**
898
899 This work was supported by National Institutes of Health grants T32-AT007533 (J.C.L.), F31-
900 AT010418 (J.C.L.), National Institutes of Health grant R01-AI117712 (R.B.L), National Science
901 Foundation grant MCB-1817955 (L.M.S.), NSF grant MCB-1817887 (R.J.D. and L.M.S.), the
902 UCSD Center for Microbiome Innovation (E.C.P.), the UCSD Ruth Stern Award (E.C.P.), NIH
903 Institutional Training grant 5 T32 GM 7240-40 (E.C.P.), and National Institutes of Health grant
904 R01GM112739-01 (N.P.K.).

905 **REFERENCES**

906 1. Laforest-Lapointe, I. & Arrieta, M. C. Microbial Eukaryotes: a Missing Link in Gut
907 Microbiome Studies. *mSystems* **3**, (2018).

908 2. Forbes, J. D., Bernstein, C. N., Tremlett, H., Van Domselaar, G. & Knox, N. C. A Fungal
909 World: Could the Gut Mycobiome Be Involved in Neurological Disease? *Front. Microbiol.*
910 **9**, 3249 (2018).

911 3. Huseyin, C. E., O'Toole, P. W., Cotter, P. D. & Scanlan, P. D. Forgotten fungi-the gut
912 mycobiome in human health and disease. *FEMS Microbiol. Rev.* **41**, 479–511 (2017).

913 4. Bergelson, J., Mittelstrass, J. & Horton, M. W. Characterizing both bacteria and fungi
914 improves understanding of the Arabidopsis root microbiome. *Sci. Rep.* **9**, 24 (2019).

915 5. Huffnagle, G. B. & Noverr, M. C. The emerging world of the fungal microbiome. *Trends*
916 *Microbiol.* **21**, 334–341 (2013).

917 6. Soverini, M. *et al.* HumanMycobiomeScan: a new bioinformatics tool for the

918 characterization of the fungal fraction in metagenomic samples. *BMC Genomics* **20**, 496
919 (2019).
920 7. Bradford, L. L. & Ravel, J. The vaginal mycobiome: A contemporary perspective on fungi
921 in women's health and diseases. *Virulence* **8**, 342–351 (2017).
922 8. Marsh, A. J., O'Sullivan, O., Hill, C., Ross, R. P. & Cotter, P. D. Sequence-based analysis
923 of the bacterial and fungal compositions of multiple kombucha (tea fungus) samples. *Food*
924 *Microbiol.* **38**, 171–178 (2014).
925 9. De Filippis, F., Laiola, M., Blaiotta, G. & Ercolini, D. Different Amplicon Targets for
926 Sequencing-Based Studies of Fungal Diversity. *Appl. Environ. Microbiol.* **83**, (2017).
927 10. Fan, D. *et al.* Activation of HIF-1α and LL-37 by commensal bacteria inhibits Candida
928 albicans colonization. *Nat. Med.* **21**, 808–814 (2015).
929 11. Jiang, T. T. *et al.* Commensal Fungi Recapitulate the Protective Benefits of Intestinal
930 Bacteria. *Cell Host Microbe* **22**, 809–816.e4 (2017).
931 12. Wheeler, M. L. *et al.* Immunological Consequences of Intestinal Fungal Dysbiosis. *Cell*
932 *Host Microbe* **19**, 865–873 (2016).
933 13. Peleg, A. Y., Hogan, D. A. & Mylonakis, E. Medically important bacterial–fungal
934 interactions. *Nat. Rev. Microbiol.* **8**, 340–349 (2010).
935 14. Mason, K. L. *et al.* Interplay between the gastric bacterial microbiota and Candida albicans
936 during postantibiotic recolonization and gastritis. *Infect. Immun.* **80**, 150–158 (2012).
937 15. Wagg, C., Schlaeppi, K., Banerjee, S., Kuramae, E. E. & van der Heijden, M. G. A. Fungal-
938 bacterial diversity and microbiome complexity predict ecosystem functioning. *Nat.*
939 *Commun.* **10**, 4841 (2019).
940 16. Durán, P. *et al.* Microbial Interkingdom Interactions in Roots Promote Arabidopsis Survival.

941 *Cell* **175**, 973–983.e14 (2018).

942 17. Tourneroche, A. *et al.* Bacterial–Fungal Interactions in the Kelp Endomicrobiota Drive
943 Autoinducer-2 Quorum Sensing. *Frontiers in Microbiology* vol. 10 (2019).

944 18. Wolfe, B. E., Button, J. E., Santarelli, M. & Dutton, R. J. Cheese Rind Communities Provide
945 Tractable Systems for In Situ and In Vitro Studies of Microbial Diversity. *Cell* **158**, 422–
946 433 (2014).

947 19. Wolfe, B. E. & Dutton, R. J. Fermented foods as experimentally tractable microbial
948 ecosystems. *Cell* **161**, 49–55 (2015).

949 20. May, A. *et al.* Kombucha: a novel model system for cooperation and conflict in a complex
950 multi-species microbial ecosystem. *PeerJ* **7**, e7565 (2019).

951 21. Morin, M., Pierce, E. C. & Dutton, R. J. Changes in the genetic requirements for microbial
952 interactions with increasing community complexity. *Elife* **7**, (2018).

953 22. Zhang, Y., Kastman, E. K., Guasto, J. S. & Wolfe, B. E. Fungal networks shape dynamics of
954 bacterial dispersal and community assembly in cheese rind microbiomes. *Nat. Commun.* **9**,
955 336 (2018).

956 23. Cleary, J. L., Kolachina, S., Wolfe, B. E. & Sanchez, L. M. Coproporphyrin III Produced by
957 the Bacterium Glutamicibacter arilaitensis Binds Zinc and Is Upregulated by Fungi in
958 Cheese Rinds. *mSystems* **3**, (2018).

959 24. Wetmore, K. M. *et al.* Rapid Quantification of Mutant Fitness in Diverse Bacteria by
960 Sequencing Randomly Bar-Coded Transposons. *MBio* **6**, (2015).

961 25. Rubin, B. E. *et al.* The essential gene set of a photosynthetic organism. *Proceedings of the*
962 *National Academy of Sciences* **112**, E6634–E6643 (2015).

963 26. Price, M. N. *et al.* Mutant phenotypes for thousands of bacterial genes of unknown function.

964 *Nature* **557**, 503–509 (2018).

965 27. Cole, B. J. *et al.* Genome-wide identification of bacterial plant colonization genes. *PLoS*
966 *Biol.* **15**, e2002860 (2017).

967 28. Hallen-Adams, H. E. & Suhr, M. J. Fungi in the healthy human gastrointestinal tract.
968 *Virulence* **8**, 352–358 (2017).

969 29. Frąc, M., Hannula, S. E., Bełka, M. & Jędryczka, M. Fungal Biodiversity and Their Role in
970 Soil Health. *Front. Microbiol.* **9**, 707 (2018).

971 30. Richards, T. A., Jones, M. D. M., Leonard, G. & Bass, D. Marine fungi: their ecology and
972 molecular diversity. *Ann. Rev. Mar. Sci.* **4**, 495–522 (2012).

973 31. Frey-Klett, P. *et al.* Ectomycorrhizal symbiosis affects functional diversity of rhizosphere
974 fluorescent pseudomonads. *New Phytol.* **165**, 317–328 (2005).

975 32. Lopez-Medina, E. *et al.* Candida albicans Inhibits Pseudomonas aeruginosa Virulence
976 through Suppression of Pyochelin and Pyoverdine Biosynthesis. *PLoS Pathog.* **11**,
977 e1005129 (2015).

978 33. Nguyen, D. D. *et al.* Indexing the Pseudomonas specialized metabolome enabled the
979 discovery of poaeamide B and the bananamides. *Nat Microbiol* **2**, 16197 (2016).

980 34. Choi, K.-H., Lee, H., Lee, S., Kim, S. & Yoon, Y. Cheese Microbial Risk Assessments - A
981 Review. *Asian-australas. J. Anim. Sci.* **29**, 307–314 (2016).

982 35. Perrin, F. *et al.* Quantitative Risk Assessment of Haemolytic and Uremic Syndrome Linked
983 to O157:H7 and Non-O157:H7 Shiga-Toxin Producing Escherichia coli Strains in Raw Milk
984 Soft Cheeses : Quantitative Risk Assessment of HUS Linked to Pathogenic STEC in
985 Cheese. *Risk Anal.* **35**, 109–128 (2015).

986 36. Ronquist, F. & Huelsenbeck, J. P. MrBayes 3: Bayesian phylogenetic inference under mixed

987 models. *Bioinformatics* **19**, 1572–1574 (2003).
988 37. Jukes, T. H. & Cantor, C. R. Evolution of protein molecules. *Mammalian protein*
989 *metabolism* (1969).
990 38. Cosetta, C. M. & Wolfe, B. E. Deconstructing and Reconstructing Cheese Rind
991 Microbiomes for Experiments in Microbial Ecology and Evolution. *Curr. Protoc. Microbiol.*
992 **56**, e95 (2020).
993 39. Conway, J. R., Lex, A. & Gehlenborg, N. UpSetR: an R package for the visualization of
994 intersecting sets and their properties. *Bioinformatics* **33**, 2938–2940 (2017).
995 40. Farris, C., Sanowar, S., Bader, M. W., Pfuetzner, R. & Miller, S. I. Antimicrobial peptides
996 activate the Rcs regulon through the outer membrane lipoprotein RcsF. *J. Bacteriol.* **192**,
997 4894–4903 (2010).
998 41. Laubacher, M. E. & Ades, S. E. The Rcs phosphorelay is a cell envelope stress response
999 activated by peptidoglycan stress and contributes to intrinsic antibiotic resistance. *J.*
1000 *Bacteriol.* **190**, 2065–2074 (2008).
1001 42. Majdalani, N., Heck, M., Stout, V. & Gottesman, S. Role of RcsF in signaling to the Rcs
1002 phosphorelay pathway in Escherichia coli. *J. Bacteriol.* **187**, 6770–6778 (2005).
1003 43. Yethon, J. A., Heinrichs, D. E., Monteiro, M. A., Perry, M. B. & Whitfield, C. Involvement
1004 of waaY, waaQ, and waaP in the Modification of Escherichia coli Lipopolysaccharide and
1005 Their Role in the Formation of a Stable Outer Membrane. *J. Biol. Chem.* **273**, 26310–26316
1006 (1998).
1007 44. Bociek, K. *et al.* Lipopolysaccharide Phosphorylation by the WaaY Kinase Affects the
1008 Susceptibility of Escherichia coli to the Human Antimicrobial Peptide LL-37. *J. Biol. Chem.*
1009 **290**, 19933–19941 (2015).

1010 45. Lofton, H., Pränting, M., Thulin, E. & Andersson, D. I. Mechanisms and fitness costs of
1011 resistance to antimicrobial peptides LL-37, CNY100HL and wheat germ histones. *PLoS One*
1012 **8**, e68875 (2013).
1013 46. Nonejuie, P., Burkart, M., Pogliano, K. & Pogliano, J. Bacterial cytological profiling rapidly
1014 identifies the cellular pathways targeted by antibacterial molecules. *Proc. Natl. Acad. Sci. U.*
1015 *S. A.* **110**, 16169–16174 (2013).
1016 47. Laich, F., Fierro, F. & Martín, J. F. Production of penicillin by fungi growing on food
1017 products: identification of a complete penicillin gene cluster in Penicillium griseofulvum
1018 and a truncated cluster in Penicillium verrucosum. *Appl. Environ. Microbiol.* **68**, 1211–1219
1019 (2002).
1020 48. Staggs, C. G., Sealey, W. M., McCabe, B. J., Teague, A. M. & Mock, D. M. Determination
1021 of the biotin content of select foods using accurate and sensitive HPLC/avidin binding. *J.*
1022 *Food Compost. Anal.* **17**, 767–776 (2004).
1023 49. Streit, W. R. & Entcheva, P. Biotin in microbes, the genes involved in its biosynthesis, its
1024 biochemical role and perspectives for biotechnological production. *Appl. Microbiol.*
1025 *Biotechnol.* **61**, 21–31 (2003).
1026 50. Hall, C. & Dietrich, F. S. The reacquisition of biotin prototrophy in Saccharomyces
1027 cerevisiae involved horizontal gene transfer, gene duplication and gene clustering. *Genetics*
1028 **177**, 2293–2307 (2007).
1029 51. Bonham, K. S., Wolfe, B. E. & Dutton, R. J. Extensive horizontal gene transfer in cheese-
1030 associated bacteria. *Elife* **6**, (2017).
1031 52. Kastman, E. K. *et al.* Biotic Interactions Shape the Ecological Distributions of
1032 Staphylococcus Species. *MBio* **7**, (2016).

1033 53. Monnet, C., Back, A. & Irlinger, F. Growth of aerobic ripening bacteria at the cheese
1034 surface is limited by the availability of iron. *Appl. Environ. Microbiol.* **78**, 3185–3192
1035 (2012).
1036 54. Blin, K. *et al.* antiSMASH 5.0: updates to the secondary metabolite genome mining
1037 pipeline. *Nucleic Acids Res.* **47**, W81–W87 (2019).
1038 55. Hantke, K. Identification of an iron uptake system specific for coprogen and rhodotorulic
1039 acid in Escherichia coli K12. *Mol. Gen. Genet.* **191**, 301–306 (1983).
1040 56. Fecker, L. & Braun, V. Cloning and expression of the fhu genes involved in iron(III)-
1041 hydroxamate uptake by Escherichia coli. *J. Bacteriol.* **156**, 1301–1314 (1983).
1042 57. Sauer, M., Hantke, K. & Braun, V. Ferric-coprogen receptor FhuE of Escherichia coli:
1043 processing and sequence common to all TonB-dependent outer membrane receptor proteins.
1044 *J. Bacteriol.* **169**, 2044–2049 (1987).
1045 58. Matzanke, B. F., Anemüller, S., Schünemann, V., Trautwein, A. X. & Hantke, K. FhuF, part
1046 of a siderophore-reductase system. *Biochemistry* **43**, 1386–1392 (2004).
1047 59. Pain, A. *et al.* Insight into the genome of Aspergillus fumigatus: analysis of a 922kb region
1048 encompassing the nitrate assimilation gene cluster. *Fungal Genet. Biol.* **41**, 443–453 (2004).
1049 60. Chryssanthou, E., Broberger, U. & Petrini, B. Malassezia pachydermatis fungaemia in a
1050 neonatal intensive care unit. *Acta Paediatr.* **90**, 323–327 (2007).
1051 61. Prohic, A., Jovovic Sadikovic, T., Krupalija-Fazlic, M. & Kuskunovic-Vlahovljak, S.
1052 Malassezia species in healthy skin and in dermatological conditions. *Int. J. Dermatol.* **55**,
1053 494–504 (2016).
1054 62. Haas, H. Fungal siderophore metabolism with a focus on Aspergillus fumigatus. *Nat. Prod.*
1055 *Rep.* **31**, 1266–1276 (2014).

1056 63. Park, M., Cho, Y.-J., Lee, Y. W. & Jung, W. H. Understanding the Mechanism of Action of
1057 the Anti-Dandruff Agent Zinc Pyrithione against Malassezia restricta. *Sci. Rep.* **8**, 12086
1058 (2018).
1059 64. Gründlinger, M. *et al.* Fungal siderophore biosynthesis is partially localized in peroxisomes.
1060 *Mol. Microbiol.* **88**, 862–875 (2013).
1061 65. Wu, G. *et al.* Genus-Wide Comparative Genomics of Malassezia Delineates Its Phylogeny,
1062 Physiology, and Niche Adaptation on Human Skin. *PLoS Genet.* **11**, e1005614 (2015).
1063 66. Triana, S. *et al.* Draft Genome Sequence of the Animal and Human Pathogen Malassezia
1064 pachydermatis Strain CBS 1879. *Genome Announc.* **3**, (2015).
1065 67. Perrin, R. M. *et al.* Transcriptional regulation of chemical diversity in Aspergillus fumigatus
1066 by LaeA. *PLoS Pathog.* **3**, e50 (2007).
1067 68. Bok, J. W. & Keller, N. P. LaeA, a regulator of secondary metabolism in Aspergillus spp.
1068 *Eukaryot. Cell* **3**, 527–535 (2004).
1069 69. Kosalková, K. *et al.* The global regulator LaeA controls penicillin biosynthesis,
1070 pigmentation and sporulation, but not roquefortine C synthesis in Penicillium chrysogenum.
1071 *Biochimie* **91**, 214–225 (2009).
1072 70. Bräse, S., Encinas, A., Keck, J. & Nising, C. F. Chemistry and biology of mycotoxins and
1073 related fungal metabolites. *Chem. Rev.* **109**, 3903–3990 (2009).
1074 71. Luckner, M. [On the synthesis of quinoline alkaloids in plants. 2. Fermentative conversion
1075 of the penicillin alkaloids cyclopenin and cyclopenol to viridicatin and viridicatol. *Eur. J.*
1076 *Biochem.* **2**, 74–78 (1967).
1077 72. Ma, Y.-M. *et al.* A new isoquinolone alkaloid from an endophytic fungus R22 of Nerium
1078 indicum. *Nat. Prod. Res.* **31**, 951–958 (2017).

1079 73. Dalsgaard, P. W. *et al.* Atlantinone A, a Meroterpenoid Produced by Penicillium ribeum and
1080 Several Cheese Associated Penicillium Species. *Metabolites* **2**, 214–220 (2012).
1081 74. Wang, X. *et al.* Chemical epigenetics alters the secondary metabolite composition of guttate
1082 excreted by an atlantic-forest-soil-derived Penicillium citreonigrum. *J. Nat. Prod.* **73**, 942–
1083 948 (2010).
1084 75. Tomoda, H. *et al.* Pyripyropenes, novel ACAT inhibitors produced by Aspergillus
1085 fumigatus. IV. Structure elucidation of pyripyropenes M to R. *J. Antibiot.* **49**, 292–298
1086 (1996).
1087 76. Patti, G. J. *et al.* A view from above: cloud plots to visualize global metabolomic data. *Anal.*
1088 *Chem.* **85**, 798–804 (2013).
1089 77. Peters, B. M., Jabra-Rizk, M. A., O'May, G. A., Costerton, J. W. & Shirtliff, M. E.
1090 Polymicrobial interactions: impact on pathogenesis and human disease. *Clin. Microbiol.*
1091 *Rev.* **25**, 193–213 (2012).
1092 78. Shirtliff, M. E., Peters, B. M. & Jabra-Rizk, M. A. Cross-kingdom interactions: Candida
1093 albicans and bacteria. *FEMS Microbiol. Lett.* **299**, 1–8 (2009).
1094 79. Scherlach, K., Graupner, K. & Hertweck, C. Molecular bacteria-fungi interactions: effects
1095 on environment, food, and medicine. *Annu. Rev. Microbiol.* **67**, 375–397 (2013).
1096 80. Wargo, M. J. & Hogan, D. A. Fungal—bacterial interactions: a mixed bag of mingling
1097 microbes. *Curr. Opin. Microbiol.* **9**, 359–364 (2006/8).
1098 81. Leclair, L. W. & Hogan, D. A. Mixed bacterial-fungal infections in the CF respiratory tract.
1099 *Med. Mycol.* **48 Suppl 1**, S125–32 (2010).
1100 82. Kim, D. *et al.* Candida albicans stimulates Streptococcus mutans microcolony development
1101 via cross-kingdom biofilm-derived metabolites. *Sci. Rep.* **7**, 41332 (2017).

1102 83. de Boer, W. & Folman, L. B. Living in a fungal world: impact of fungi on soil bacterial
1103 niche development. *FEMS microbiology* (2005).
1104 84. Johansson, J. F., Paul, L. R. & Finlay, R. D. Microbial interactions in the mycorrhizosphere
1105 and their significance for sustainable agriculture. *FEMS Microbiol. Ecol.* **48**, 1–13 (2004).
1106 85. Tarkka, M. T., Sarniguet, A. & Frey-Klett, P. Inter-kingdom encounters: recent advances in
1107 molecular bacterium-fungus interactions. *Curr. Genet.* **55**, 233–243 (2009).
1108 86. Moree, W. J. *et al.* Interkingdom metabolic transformations captured by microbial imaging
1109 mass spectrometry. *Proc. Natl. Acad. Sci. U. S. A.* **109**, 13811–13816 (2012).
1110 87. Clancy, A. *et al.* Evidence for siderophore-dependent iron acquisition in group B
1111 streptococcus. *Mol. Microbiol.* **59**, 707–721 (2006).
1112 88. Jin, B. *et al.* Iron acquisition systems for ferric hydroxamates, haemin and haemoglobin in
1113 Listeria monocytogenes. *Mol. Microbiol.* **59**, 1185–1198 (2006).
1114 89. Sheldon, J. R. & Heinrichs, D. E. Recent developments in understanding the iron acquisition
1115 strategies of gram positive pathogens. *FEMS Microbiol. Rev.* **39**, 592–630 (2015).
1116 90. Arias, A. A. *et al.* Growth of desferrioxamine-deficient Streptomyces mutants through
1117 xenosiderophore piracy of airborne fungal contaminations. *FEMS Microbiol. Ecol.* **91**,
1118 (2015).
1119 91. Mishra, R. P. N. *et al.* Staphylococcus aureus FhuD2 is involved in the early phase of
1120 staphylococcal dissemination and generates protective immunity in mice. *J. Infect. Dis.* **206**,
1121 1041–1049 (2012).
1122 92. Li, H. *et al.* The outer mucus layer hosts a distinct intestinal microbial niche. *Nat. Commun.*
1123 **6**, 8292 (2015).
1124 93. Rocha, E. R. & Krykunivsky, A. S. Anaerobic utilization of Fe(III)-xenosiderophores

among Bacteroides species and the distinct assimilation of Fe(III)-ferrichrome by Bacteroides fragilis within the genus. *Microbiologyopen* **6**, (2017).

94. Emri, T. *et al.* Towards high-siderophore-content foods: optimisation of coprogen production in submerged cultures of Penicillium nalgiovense. *J. Sci. Food Agric.* **93**, 2221–2228 (2013).

95. Ong, S. A. & Neilands, J. B. Siderophores in microbially processed cheese. *J. Agric. Food Chem.* **27**, 990–995 (1979).

96. David, L. A. *et al.* Diet rapidly and reproducibly alters the human gut microbiome. *Nature* **505**, 559–563 (2014).

97. Rehner, S. A. & Samuels, G. J. Molecular systematics of the Hypocreales: a teleomorph gene phylogeny and the status of their anamorphs. *Can. J. Bot.* **73**, 816–823 (1995).

98. Glass, N. L. & Donaldson, G. C. Development of primer sets designed for use with the PCR to amplify conserved genes from filamentous ascomycetes. *Appl. Environ. Microbiol.* **61**, 1323–1330 (1995).

99. Dunnett, C. W. A Multiple Comparison Procedure for Comparing Several Treatments with a Control. *J. Am. Stat. Assoc.* **50**, 1096–1121 (1955).

100. Wickham, H. ggplot2: Elegant Graphics for Data Analysis. (2009).

101. Cleary, J. L., Luu, G. T., Pierce, E. C., Dutton, R. J. & Sanchez, L. M. BLANKA: an Algorithm for Blank Subtraction in Mass Spectrometry of Complex Biological Samples. *J. Am. Soc. Mass Spectrom.* **30**, 1426–1434 (2019).

102. Mohimani, H. *et al.* Dereplication of microbial metabolites through database search of mass spectra. *Nature Communications* vol. 9 (2018).

103. Mohimani, H. *et al.* Dereplication of peptidic natural products through database search of

1148 mass spectra. *Nat. Chem. Biol.* **13**, 30–37 (2017).

1149 104. Shannon, P. *et al.* Cytoscape: a software environment for integrated models of biomolecular
1150 interaction networks. *Genome Res.* **13**, 2498–2504 (2003).

1151 105. Tang, Y., Horikoshi, M. & Li, W. ggfortify: Unified Interface to Visualize Statistical Result
1152 of Popular R Packages. *The R Journal* vol. 8 (2016).

1153 106. Huerta-Cepas, J. *et al.* eggNOG 5.0: a hierarchical, functionally and phylogenetically
1154 annotated orthology resource based on 5090 organisms and 2502 viruses. *Nucleic Acids Res.*
1155 **47**, D309–D314 (2019).

1156 107. Baba, T. *et al.* Construction of Escherichia coli K-12 in-frame, single-gene knockout
1157 mutants: the Keio collection. *Mol. Syst. Biol.* **2**, 2006.0008 (2006).

1158 108. Schindelin, J. *et al.* Fiji: an open-source platform for biological-image analysis. *Nat.*
1159 *Methods* **9**, 676–682 (2012).

1160 109. Grenier, F., Matteau, D., Baby, V. & Rodrigue, S. Complete Genome Sequence of
1161 Escherichia coli BW25113. *Genome Announc.* **2**, (2014).

1162 110. Lawrence, M. *et al.* Software for computing and annotating genomic ranges. *PLoS Comput.*
1163 *Biol.* **9**, e1003118 (2013).

1164 111. Love, M. I., Huber, W. & Anders, S. Moderated estimation of fold change and dispersion
1165 for RNA-seq data with DESeq2. *Genome Biol.* **15**, 550 (2014).

1166 112. Datsenko, K. A. & Wanner, B. L. One-step inactivation of chromosomal genes in
1167 Escherichia coli K-12 using PCR products. *Proc. Natl. Acad. Sci. U. S. A.* **97**, 6640–6645
1168 (2000).

1169 113. Koren, S. *et al.* Canu: scalable and accurate long-read assembly via adaptive k-mer
1170 weighting and repeat separation. *Genome Res.* **27**, 722–736 (2017).

1171 114. Vaser, R., Sović, I., Nagarajan, N. & Šikić, M. Fast and accurate de novo genome assembly
1172 from long uncorrected reads. *Genome Res.* **27**, 737–746 (2017).
1173 115. Walker, B. J. *et al.* Pilon: an integrated tool for comprehensive microbial variant detection
1174 and genome assembly improvement. *PLoS One* **9**, e112963 (2014).
1175 116. Min, B., Grigoriev, I. V. & Choi, I.-G. FunGAP: Fungal Genome Annotation Pipeline using
1176 evidence-based gene model evaluation. *Bioinformatics* **33**, 2936–2937 (2017).
1177 117. Jones, P. *et al.* InterProScan 5: genome-scale protein function classification. *Bioinformatics*
1178 **30**, 1236–1240 (2014).
1179 118. Lim, F. Y., Sanchez, J. F., Wang, C. C. C. & Keller, N. P. Toward awakening cryptic
1180 secondary metabolite gene clusters in filamentous fungi. *Methods Enzymol.* **517**, 303–324
1181 (2012).
1182 119. Xie, C. *et al.* KOBAS 2.0: a web server for annotation and identification of enriched
1183 pathways and diseases. *Nucleic Acids Res.* **39**, W316–22 (2011).
1184 120. The Gene Ontology Consortium. The Gene Ontology Resource: 20 years and still GOing
1185 strong. *Nucleic Acids Res.* **47**, D330–D338 (2019).
1186 121. Ashburner, M. *et al.* Gene ontology: tool for the unification of biology. The Gene Ontology
1187 Consortium. *Nat. Genet.* **25**, 25–29 (2000).

1188 **SUPPLEMENTAL FIGURE AND TABLE LEGENDS**
1189
1190 **Supplementary Figure 1**: **Impacts of fungal species on bacterial growth after 7 days of co-**
1191 **culture on cheese curd agar, pH 7**. CFU: colony forming units. N=3, error bars show standard
1192 deviation and black point is the mean. * represents a significant difference in bacterial growth in
1193 the presence of the fungal partner relative to alone (two-sided Dunnett's test, p-value <.05).
1194
1195 **Supplementary Figure 2**: **Impacts of bacterial species on fungal growth after 7 days of co-**
1196 **culture on cheese curd agar, pH 7**. For filamentous fungi, spore counts were used as a proxy
1197 for fungal CFUs. N=3, error bars show standard deviation and black point is the mean. *
1198 represents a significant difference in fungal growth in the presence of the bacterial partner

1199 relative to alone (two-sided Dunnett's test, p-value <.05).
1200
1201 **Supplementary Figure 3: RB-TnSeq assay.** Characterized pooled bacterial mutant libraries
1202 were grown in a biofilm either alone or in a mixed biofilm with a fungal partner. After seven
1203 days of growth, mutant abundances were compared to the starting library abundances for each
1204 condition. Changes in barcode abundances were used to calculate gene fitness values. Genes
1205 with fitness values that differed significantly between co-culture and alone conditions
1206 (significant interaction fitness) were identified as potentially relevant to fungal interaction.
1207
1208 **Supplementary Figure 4: COG categories of genes with interaction fitness.** Number of genes
1209 with interaction fitness falling into each COG category for *E. coli* (left) or *P. psychrophila*
1210 (right).
1211
1212 **Supplementary Figure 5: Bacterial Cytological Profiling of △*tolC E.coli* treated with**
1213 **known antibiotic compounds on cheese curd agar.** DAPI dye stains DNA and FM4-64 dye
1214 stains bacterial membranes. SYTOX green stains nucleic acids but cannot penetrate live cells.
1215 Scale bars represent 2 μm.
1216
1217 **Supplementary Figure 6**: **Siderophore production by filamentous molds.** Liquid CAS assay
1218 was performed on filtered and concentrated fungal supernatants from three replicates grown in
1219 liquid cheese for 12 days. Row A) 1-3: Liquid cheese control 4-6: *Penicillium* SAM3. Row B) 1-
1220 3: *Debaryomyces* 135B 4-6: *Penicillium* #12. Row C) 1-3: *Candida* 135E. 4-6: *Penicillium*
1221 RS17. Row D) 1-3: *Scopulariopsis* 165-5 Row E) 1-3: *Scopulariopsis* JB370. Row F) 1-3:
1222 *Fusarium* 554A. % Siderophore units calculated as $[(A_r - A_s)/(A_r)]*100$, where A_r is the
1223 absorbance of the cheese curd agar supernatant blank and A_s is the absorbance of the sample.
1224 N=3, error bars show standard deviation and black point is the mean.
1225
1226 **Supplementary Figure 7**: **Fitness defect of *fep* mutants on iron-limiting CCA.** Visual assays
1227 of *E. coli* mutant growth spotted alone on CCA pH 7.
1228
1229 **Supplementary Figure 8. Deletion of *laeA* gene in *Penicillium* sp. str. #12**. A. Schematic
1230 representation of the genetic construct for *laeA* deletion in *Penicillium* sp. str. #12. The construct
1231 is constituted of the *hph* gene conferring resistance to hygromycin. The positions of the
1232 restriction enzyme cutting sites are shown on the map. B. Southern blot analyses of genomic
1233 DNA from the WT and the Δ*laeA* strains. Ten micrograms of total DNA from each strain was
1234 digested with the appropriate enzymes and subjected to Southern blot analysis using respectively
1235 the 5' flank fragment (blue) and the 3'fragment (grey) as probes. The 1 Kb DNA ladder from
1236 New England Biolabs was used to determine the size of the expected bands. The blot image was
1237 cropped to place the confirmed mutant adjacent to the positive control. The transformants that
1238 were confirmed to not have the correct insertion were not included in the figure.
1239

1240 **Supplementary Data 1: RB-TnSeq fitness values for *E. coli* grown with fungal partners**
1241 **compared to alone.**
1242
1243 **Supplementary Data 2: RB-TnSeq fitness values for *P. psychrophila* grown with fungal**
1244 **partners compared to alone.**
1245
1246 **Supplementary Data 3: Genes with significant interaction fitness for *E. coli* grown with**
1247 **fungal partners.**
1248
1249 **Supplementary Data 4: Genes with significant interaction fitness for *P. psychrophila* grown**
1250 **with fungal partners.**
1251
1252 **Supplementary Data 5: Intersection lists for *E. coli* genes with interaction fitness across all**
1253 **conditions.**
1254
1255 **Supplementary Data 6: Intersection lists for *P. psychrophila* genes with interaction fitness**
1256 **across all conditions.**
1257
1258 **Supplementary Data 7: Functional enrichment results for *E. coli* genes with interaction**
1259 **fitness across all conditions.**
1260
1261 **Supplementary Data 8: Functional enrichment results for *P. psychrophila* genes with**
1262 **interaction fitness across all conditions.**
1263
1264 **Supplementary Data 9: RNA-Seq differential expression analysis for *E. coli* grown with**
1265 ***Penicillium* sp. str. #12 (*E. coli* perspective, alone condition as reference).**
1266
1267 **Supplementary Data 10: Iron-related genes that are differentially expressed by *E. coli***
1268 **when grown with *Penicillium* sp. str. #12 relative to *E. coli* growth alone.**
1269
1270 **Supplementary Data 11: Metabolite production by Δ*laeA* and WT *Penicillium* sp. str. #12.**
1271 **Δ*laeA* used as the reference condition.**
1272
1273 **Supplementary Data 12: RB-TnSeq fitness values for *E. coli* grown with Δ*laeA* or WT**
1274 ***Penicillium* sp. str. #12 compared to alone.**
1275
1276 **Supplementary Data 13: RNA-Seq differential expression analysis for Δ*laeA* vs. WT**
1277 ***Penicillium* sp. str. #12 (WT used as the reference condition).**
1278
1279 **Supplementary Data 14: Functional enrichment results for genes differentially expressed in**
1280 **Δ*laeA* vs. WT *Penicillium* sp. str. #12.**
1281
1282 **Supplementary Data 15: Overlap of *E. coli* or *P. psychrophila* genes with interaction fitness.**
1283
1284

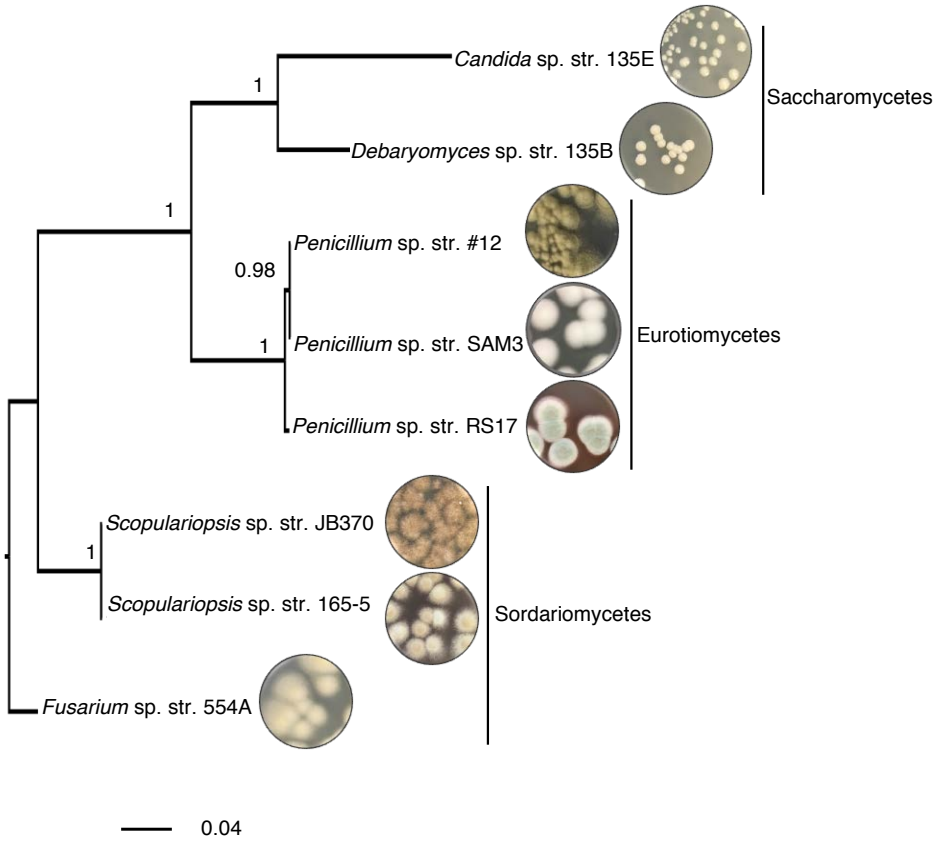

Figure 1: Fungal interaction partners span the phylogenetic and morphological diversity of the cheese ecosystem. Phylogenetic tree based on large subunit rRNA of the cheese fungi used as interaction partners in this study. The tree was built using Bayesian phylogenetic inference with MrBayes[36] and the Jukes and Cantor substitution model[37]. Branch labels display posterior probability.

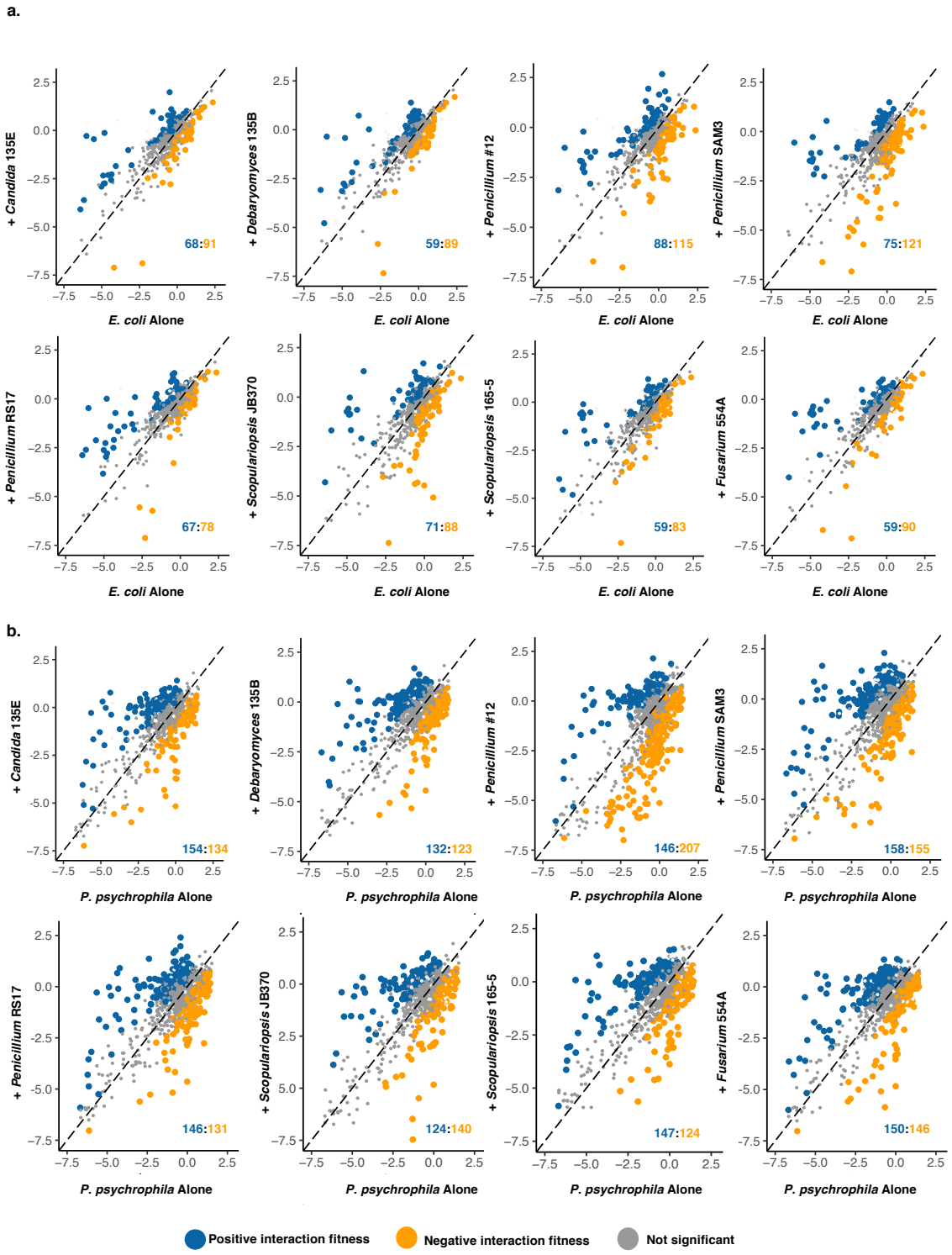

Figure 2: Bacterial genes with significant interaction fitness across fungal partners. Each dot represents a gene, with colored dots indicating genes with a significant interaction fitness. X

and Y values indicate gene fitness values in each condition (alone on x-axis versus grown with a fungal partner on y-axis), and the colored numbers in the lower right hand corner indicate how many genes have either positive (blue) or negative (orange) interaction fitness. **a,** *E. coli.* **b,** *P. psychrophila.*

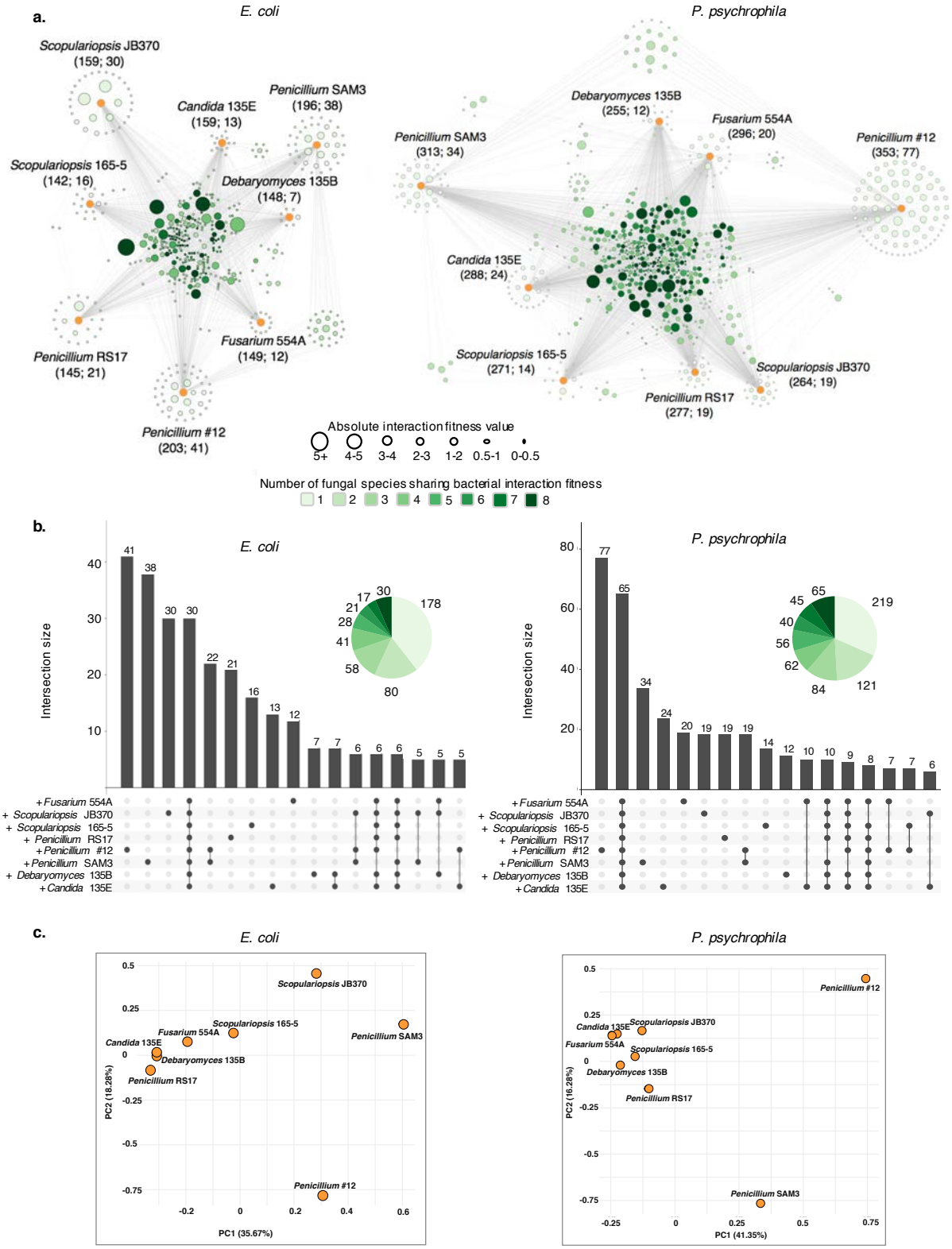

Figure 3: Bacterial genes with differential fitness in the presence of fungi. **a,** Network of *E. coli* (left) or *P. psychrophila* (right) genes with an interaction fitness based on RB-TnSeq. Each

orange node represents a fungal partner and is labeled as follows: Fungal partner (Number of genes with interaction fitness; Number of genes with interaction fitness unique to this condition). Each green node represents a bacterial gene. Green nodes are shaded by the number of fungal conditions in which this gene has an interaction fitness as shown in the legend below and are sized by average strength of interaction fitness across partners. **b,** UpSet[39] plots showing the overlaps, or intersections, of *E. coli* (left) or *P. psychrophila* (right) gene sets with interaction fitness across fungal partners. These UpSet plots are conceptually similar to Venn Diagrams. The connected circles indicate which fungal conditions are included in the intersection, and the size of the intersection (the number of genes that have an interaction fitness in all the highlighted conditions) is displayed in the main bar chart. Intersections <5 genes are not shown. For example, in the *E. coli* panel, 30 genes have an interaction fitness with all partners (all fungi circles are connected), while 22 other genes have an interaction fitness with *Penicillium* sp. str. #12 and with *Penicillium* sp. str. SAM3 (only *Penicillium* sp. str. #12 *and Penicillium* sp. str. SAM3 circles are connected). **c,** PCA of the raw fitness values for all *E. coli* (left) or *P. psychrophila* (right) genes with an interaction fitness in at least one fungal condition.

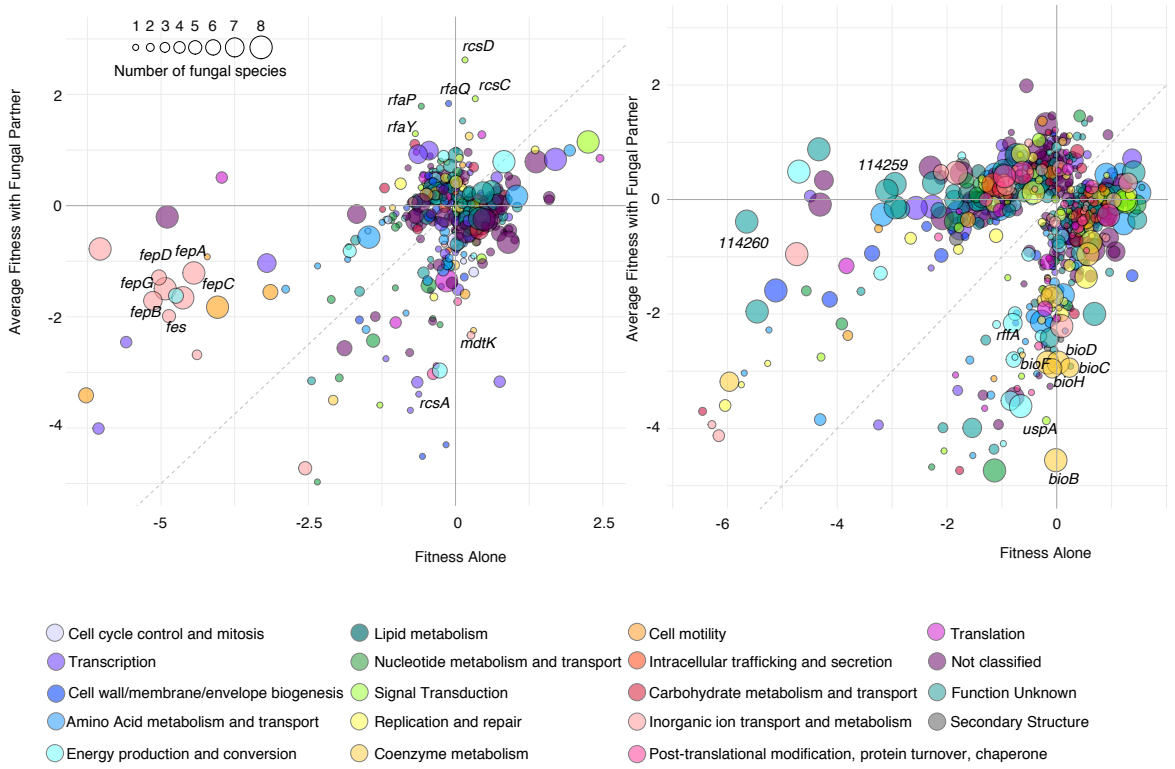

Figure 4: Functional analysis of the bacterial genes associated with interaction fitness. Comparison of *E. coli* (left) or *P. psychrophila* (right) gene fitness values alone compared to fitness values with a fungal partner, colored by COG category and sized by the conservation of effect among fungal partners (1-8 fungal species). Genes discussed in the text are labeled with the gene name.

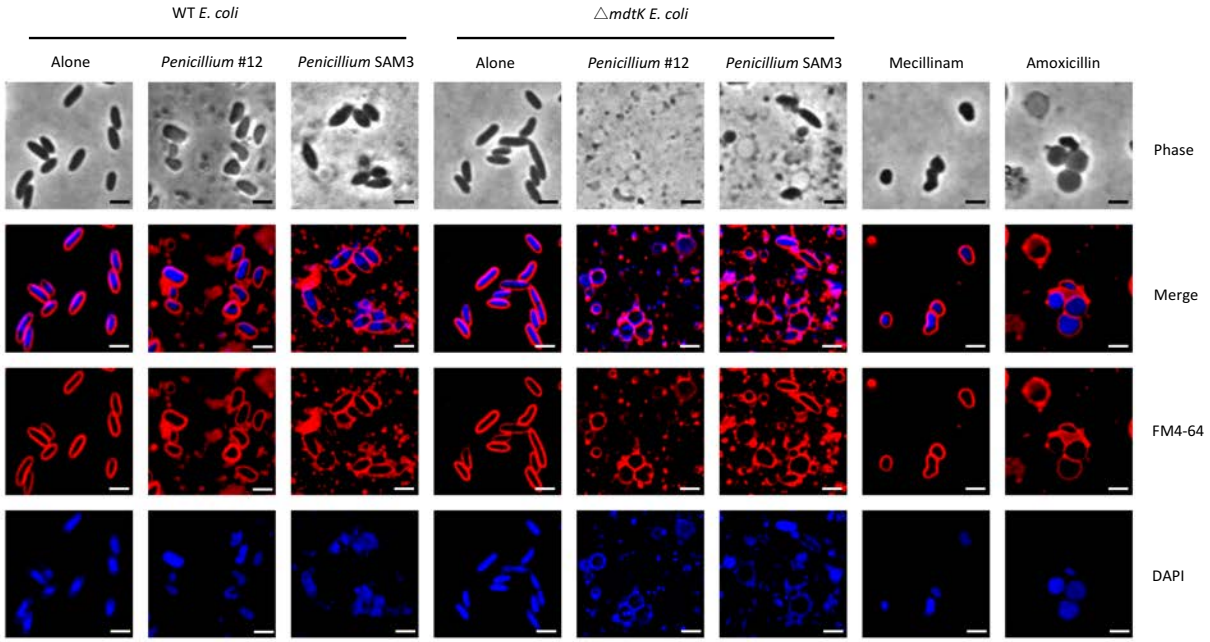

1429
1430
1431 **Figure 5: Bacterial cytological profiling of *E. coli* grown in a mixed biofilm with *Penicillium***
1432 **sp. str. #12 and *Penicillium* sp. str. SAM3 on CCA plates.** The phenotype of *E. coli* grown
1433 with these fungi is similar to that seen when *E. coli* is exposed to antibiotics targeting cell wall
1434 biosynthesis. DAPI dye stains DNA and FM4-64 dye stains bacterial membranes. Scale bars
1435 represent 2 μm.
1436
1437
1438
1439
1440
1441
1442
1443
1444
1445
1446
1447
1448
1449
1450
1451
1452
1453
1454
1455
1456

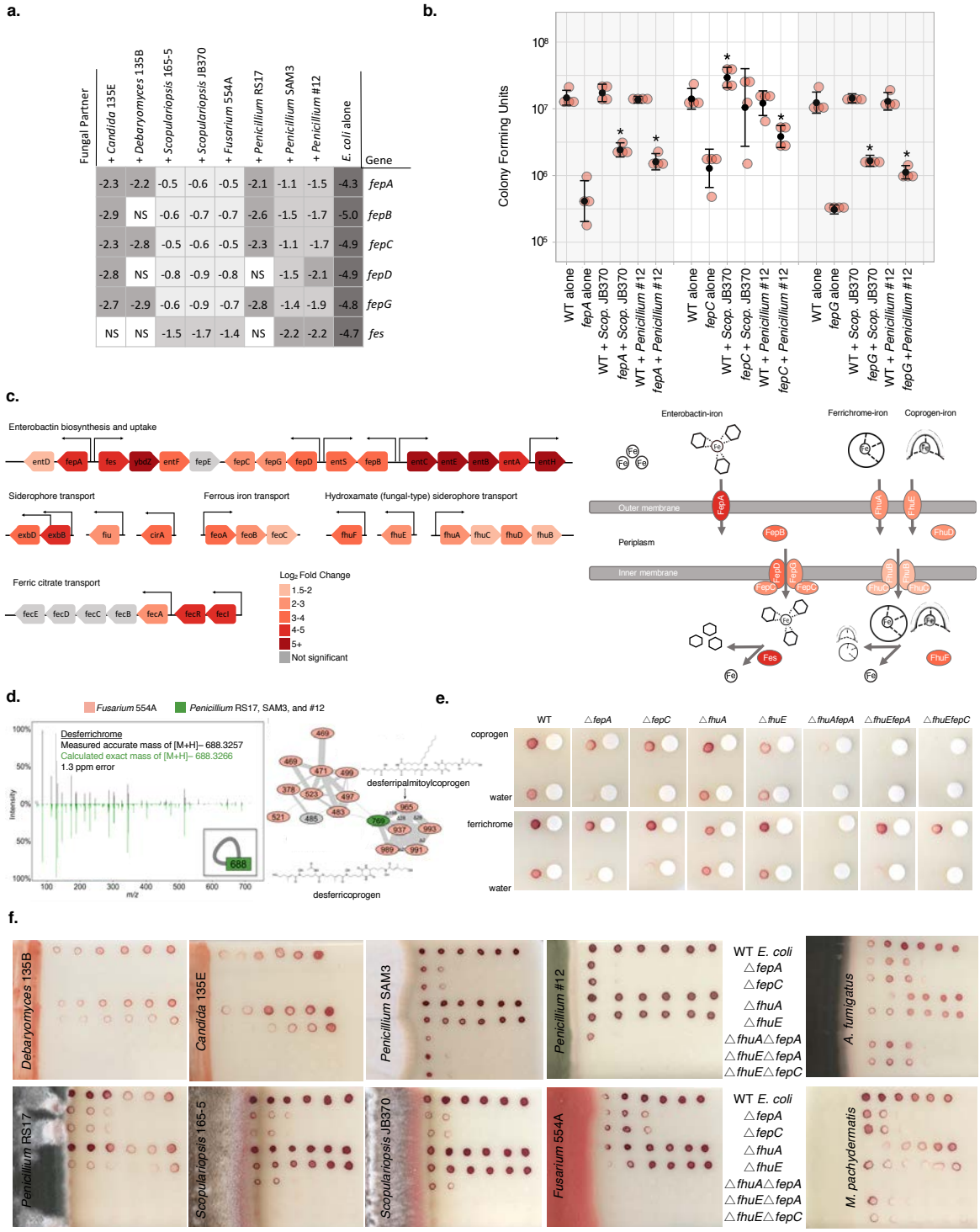

Figure 6: Utilization of fungal siderophores by *E. coli*. a, RB-TnSeq fitness values for *fep* operon genes in alone or interactive conditions, showing an increase in fitness in the presence of fungal species. NS- not significant. **b,** Colony forming units of WT and Δ*fep* mutants after 7 days of 1:1 competitive growth on CCA. Competitions were performed either alone or with

Penicillium sp. str. #12 or *Scopulariopsis* sp. str. JB370. N=4, error bars show standard deviation. Asterisk indicates significantly different growth in the presence of a fungus relative to growth alone (two-sided two-sample equal variance t-test p-value < 0.05). **c,** *E. coli* iron-related genes upregulated in the presence of *Penicillium* sp. str. #12. Significance cutoff made at abs($\log_2$(fold-change)) >1.5 and adjusted p-value <0.05. **d,** Fungal siderophores identified by mass spectrometry. Inset on the left shows the node that represents the desferrichrome fragmentation pattern depicted while network on the right represents coprogen-related molecules. Coprogen B and ferrichrome were found by matching fragmentation patterns to library spectra. Both identifications were confirmed using retention time and fragmentation matching to a purchased standard. **e,** Visual assays of *Δfep* mutant growth with purified siderophores coprogen and ferrichrome. **f,** Visual assays of *E. coli* mutant growth at varying distances from pre-cultured cheese fungi, *A. fumigatus* (soil, human pathogen), and *M. pachydermatis* (skin commensal). Growth performed on CCA containing tetrazolium chloride (red growth indicator).

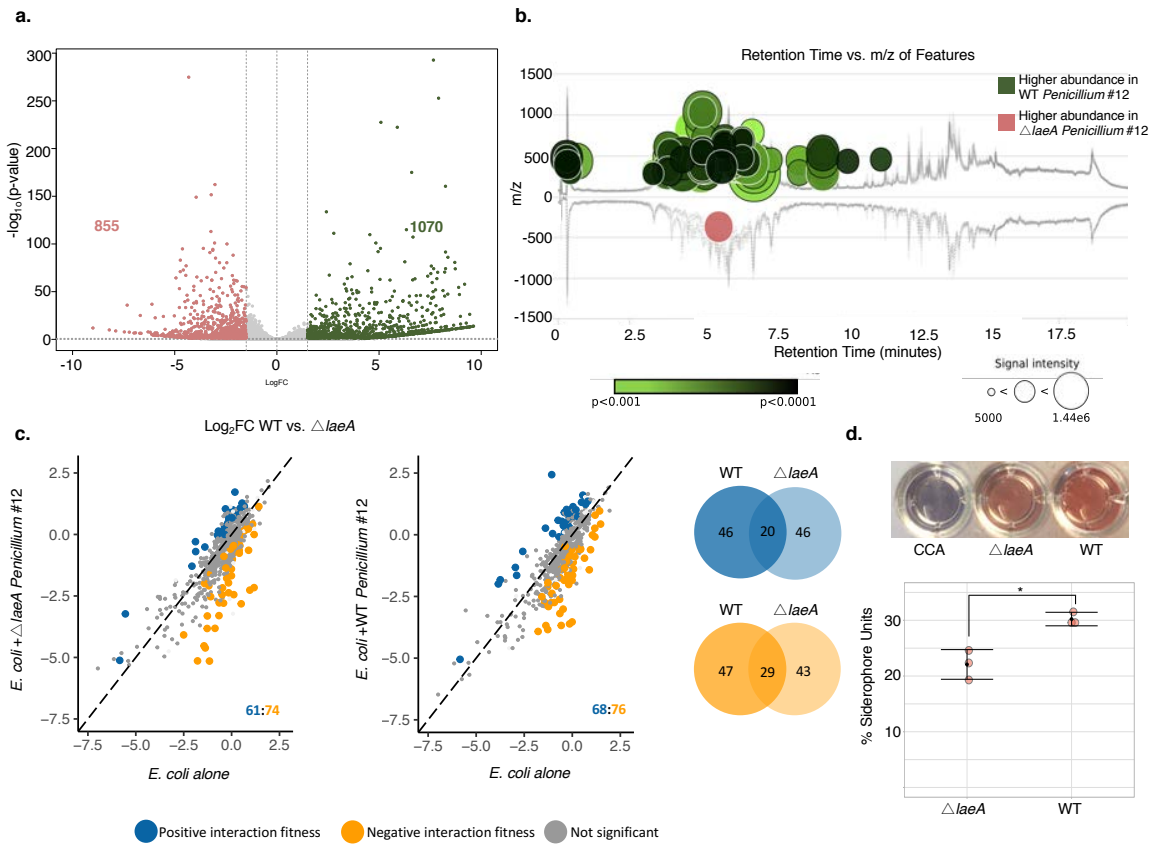

Figure 7: Fungal metabolite production impacts bacterial-fungal interactions. a, Differential expression of WT *Penicillium* sp. str. #12 relative to Δ*laeA* after three days of growth on CCA. Labeled on the volcano plot are the number of genes with a $\log_2$FC of >1.5 (green) or <-1.5 (red) and adjusted p-value of <0.05. **b,** The metabolomics data analysis platform XCMS[76] was used to compare features detected by LC-MS analyses of Δ*laeA* and WT *Penicillium* sp. str. #12 extracts. Features of higher abundance in WT relative to Δ*laeA* are depicted as green nodes on the top of the mirror plot and features of lower abundance in WT relative to Δ*laeA* are depicted as red nodes on the bottom. Node radius is proportional to the fold change of the detected features and color intensity is dependent on p-value. The graph displays only those features with a p-value less than or equal to 0.05, fold change higher than or equal to 10, *m/z* between 200 and 2000 Da, and intensity higher than 500. **c,** *E. coli* genes with significant interaction fitness with Δ*laeA* and WT *Penicillium* sp. str. #12. Each dot represents a gene, with colored dots indicating genes with interaction fitness. X and Y values (alone on x-axis and +fungal partner on y-axis) indicate gene fitness values in each condition, and the numbers in the lower right hand corner indicate how many genes have either positive (blue) or negative (orange) interaction fitness. Venn diagrams display the overlap of these gene sets. **d,** Liquid CAS assay of supernatants from blank control CCA medium, Δ*laeA,* or WT *Penicillium* sp. str. #12. N=3, error bars show standard deviation from the mean. Asterisk indicates significantly different siderophore production (two-sided two-sample equal variance t-test p-value 0.009).